Distinct release properties of glutamate/GABA co-transmission serve as a frequency-dependent filtering of supramammillary inputs

Himawari Hirai[1], Kohtaro Konno[2], Miwako Yamasaki[2], Masahiko Watanabe[2], Takeshi Sakaba[1], Yuki Hashimotodani[1*]

[1]Graduate School of Brain Science, Doshisha University, Kyoto 610-0394, Japan
[2]Department of Anatomy, Faculty of Medicine, Hokkaido University, Sapporo, Japan

*To whom correspondence should be addressed:
Yuki Hashimotodani, PhD
Graduate School of Brain Science
Doshisha University
1-3 Tatara Miyakodani, Kyotanabe, Kyoto
610-0394, Japan
Phone: +81-774-65-6057
E-mail: hashimotodani@gmail.com

Abstract

Glutamate and GABA co-transmitting neurons exist in several brain regions; however, the mechanism by which these two neurotransmitters are co-released from the same synaptic terminals remains unclear. Here, we show that the supramammillary nucleus (SuM) to dentate granule cell synapses, which co-release glutamate and GABA, exhibit differences between glutamate and GABA release properties in paired-pulse ratio, Ca^{2+}-sensitivity, presynaptic receptor modulation, and Ca^{2+} channel-vesicle coupling configuration. Moreover, uniquantal synaptic responses show independent glutamatergic and GABAergic responses. Morphological analysis reveals that most SuM boutons form distinct glutamatergic and GABAergic synapses in proximity, each characterized by GluN1 and $GABA_A\alpha1$ labeling, respectively. Notably, glutamate/GABA co-transmission exhibits distinct short-term plasticities, with frequency-dependent depression of glutamate and frequency-independent stable depression of GABA. Our findings suggest that glutamate and GABA are co-released from different synaptic vesicles within the SuM terminals, and reveal that distinct transmission modes of glutamate/GABA co-release serve as frequency-dependent filters of SuM inputs.

Introduction

Despite the classical view of Dale's Principle known as "one neuron, one transmitter": a single neuron releases a single neurotransmitter (Eccles et al., 1954), a growing body of evidence has demonstrated that many types of neurons in several brain regions co-release multiple neurotransmitters including classical neurotransmitters (glutamate, GABA, glycine, and acetylcholine), monoamines, purins, and neuropeptides (Hnasko and Edwards, 2012; Vaaga et al., 2014; Trudeau and El Mestikawy, 2018; Wallace and Sabatini, 2023). While this co-release is thought to contribute to several brain functions (Nusbaum et al., 2001; Trudeau et al., 2014; Tritsch et al., 2016; Ma et al., 2018; Kim and Sabatini, 2023), little is known about the functional implications of the co-release of two or more neurotransmitters into neural circuits and the molecular mechanisms of how multiple neurotransmitters are co-transmitted. Here, we define co-release as the release of multiple neurotransmitters from a single neuron, regardless of whether the neurotransmitters are packaged in the same or different synaptic vesicles, and co-transmission as synaptic transmission occurring by multiple neurotransmitters and detected by distinct postsynaptic receptors (Wallace and Sabatini, 2023).

The co-release of glutamate and GABA, both fast-acting and functionally opposing neurotransmitters, has recently been identified in several brain regions of the adult brain (Trudeau and El Mestikawy, 2018; Kim and Sabatini, 2023; Wallace and Sabatini, 2023). In particular, the lateral habenula and dentate gyrus (DG) of the hippocampus have been extensively studied for the co-release of glutamate and GABA. The lateral habenula neurons receive glutamate/GABA co-releasing synaptic inputs from the entopeduncular nucleus (EP) (Shabel et al., 2014; Wallace et al., 2017; Root et al., 2018) and ventral tegmental area (VTA) (Root et al., 2014; Yoo et al., 2016; Root et al., 2018). Hypothalamic supramammillary nucleus (SuM) neurons projecting to the DG also co-release glutamate and GABA (Pedersen et al., 2017; Hashimotodani et al., 2018; Billwiller et al., 2020; Chen et al., 2020; Li et al., 2020; Ajibola et al., 2021). To understand how synaptic inputs mediated by the co-release of the excitatory action of glutamate and the inhibitory action of GABA are integrated and impact postsynaptic cells, it is necessary to elucidate how glutamate and GABA are co-released from the synaptic terminals. Mechanistically, if glutamate and GABA are co-released from distinct vesicle populations, each release could be differently regulated by distinct release mechanisms. Such distinct co-release modes of glutamate and GABA are expected to implement different presynaptic plasticity, which will have diverse effects on postsynaptic neurons in response to different activity patterns. By contrast, if two neurotransmitters are co-released from the same

synaptic vesicles, both glutamate and GABA release are expected to be under the same regulation.

Whether glutamate and GABA are packaged in the same or separate vesicles remains controversial. Electrophysiological studies have demonstrated the co-packaging of glutamate and GABA in the same synaptic vesicles at EP-lateral habenular synapses (Shabel et al., 2014; Kim et al., 2022). Conversely, an immunoelectron microscopy (immuno EM) study demonstrated that glutamatergic and GABAergic vesicle populations are segregated in the axon terminals of the EP and VTA projections in the lateral habenula, and that single terminals form both excitatory and inhibitory synapses (Root et al., 2018). The same study also reported segregated vesicle populations of glutamate and GABA in the axon terminals of the SuM projections in the DG (Root et al., 2018). However, the mode of co-release of glutamate and GABA from the SuM terminals has never been functionally addressed.

In this study, we investigated the release properties of glutamate/GABA co-transmission at SuM-granule cell (GC) synapses. We demonstrate that glutamate/GABA co-transmission shows independent synaptic responses and differential short-term plasticity and that their postsynaptic targets are segregated. Our results suggest that the segregation of two different populations of transmitters makes it possible to exert short-term dynamic changes in the co-transmission balance of glutamate and GABA and modulate GC activity in a frequency-dependent manner.

Results

Glutamate/GABA co-transmission shows different release probabilities and Ca^{2+} sensitivities

To optogenetically stimulate SuM inputs in the DG, channelrhodopsin-2 (ChR2) was expressed in SuM neurons by injecting a Cre-dependent adeno-associated virus (AAV) encoding ChR2-eYFP (AAV-DIO-ChR2(H134R)-eYFP) into the lateral SuM of vesicular glutamate transporter 2 (VGluT2)-Cre mice (Hashimotodani et al., 2018; Hirai et al., 2022; Tabuchi et al., 2022) (Figures 1 A and 1B). Consistent with previous reports (Boulland et al., 2009; Soussi et al., 2010; Root et al., 2018; Billwiller et al., 2020; Ajibola et al., 2021), the vast majority of ChR2-eYFP-expressing SuM boutons in the DG co-expressed VGluT2 and vesicular GABA transporter (vesicular inhibitory amino acid transporter, VIAAT) (Figures 1C-1E). We performed whole-cell patch-clamp recordings from GCs in acute hippocampal slices and recorded optically evoked excitatory or inhibitory postsynaptic currents (EPSCs or IPSCs) at SuM-GC synapses in the presence of picrotoxin or NBQX/D-AP5, respectively. To examine

115 whether the co-release of glutamate and GABA exhibits the same or different release properties,
116 we first monitored the paired-pulse ratio (PPR), an index of the change in presynaptic
117 transmitter release (Zucker and Regehr, 2002), of glutamate/GABA co-transmission by paired
118 stimulation (inter-stimulus interval: 100 ms). As reported previously (Hashimotodani et al.,
119 2018; Tabuchi et al., 2022), both EPSCs and IPSCs at SuM-GC synapses exhibited paired-
120 pulse depression (Figure 1F). Importantly, we found that PPR was significantly different
121 between EPSCs and IPSCs; EPSCs were more depressed than IPSCs (Figure 1G) (EPSC: 0.46
122 ± 0.03, n = 8; IPSC: 0.6 ± 0.03, n = 8, $p < 0.01$, unpaired t test). It is possible that direct
123 illumination of presynaptic boutons could increase transmitter release due to the broadening of
124 the presynaptic waveform or direct influx of Ca^{2+} through ChR2 (Jackman et al., 2014; Rost et
125 al., 2022). To avoid this possibility, we stimulated SuM axons instead of SuM terminals
126 (Supplementary Figures 1A and 1B), and obtained similar results to terminal illumination
127 (Supplementary Figure 1C-F). Altogether, these results suggest that the release probability
128 differs between the co-released glutamate and GABA from SuM terminals in the DG.
129 Since vesicular exocytosis depends on the extracellular Ca^{2+} concentration, we next
130 examined whether reducing the release probability by lowering the extracellular Ca^{2+}
131 concentration could have different effects on glutamate/GABA co-transmission. Reducing
132 extracellular Ca^{2+} concentration from 2.5 to 1 mM decreased the amplitudes of EPSCs and
133 IPSCs (Figure 1H) (EPSC: n = 14, $p < 0.001$, paired t test; IPSC: n = 15, $p < 0.001$, paired t
134 test). Remarkably, IPSCs decreased to a greater extent than EPSCs (Figure 1I) (EPSC: 45.1 ±
135 4.1% of reduction, n = 14; IPSC: 58.2 ± 2.7% of reduction, n = 15, $p < 0.01$, unpaired t test),
136 suggesting different Ca^{2+} sensitivities for glutamate and GABA release.
137
138 **Co-release of glutamate and GABA differs in presynaptic modulation and Ca^{2+} channel-**
139 **vesicle coupling configuration**
140 To further investigate whether the release properties of glutamate and GABA at SuM-GC
141 synapses are different, we next examined whether glutamate and GABA co-release are
142 mediated by different types of Ca^{2+} channels. We found that the application of ω-conotoxin-
143 GVIA (ω-CgTx), an N-type Ca^{2+} channel blocker, had no effect on EPSCs or IPSCs at SuM-
144 GC synapses (Figure 2A) (EPSC: 92.5 ± 13.8% of baseline, n = 6, p = 0.53, Wilcoxon signed-
145 rank test; IPSC: 101.7 ± 11% of baseline, n = 6, p = 0.89, paired t test). We confirmed that ω-
146 CgTx inhibited CA3-CA1 transmission (Supplementary Figure 2) (Wu and Saggau, 1994),
147 suggesting that ω-CgTx we used is effective. In contrast, the application of ω-agatoxin-IVA
148 (ω-Aga-IVA), a P/Q-type Ca^{2+} channel blocker, suppressed both EPSCs and IPSCs to the same

extent at SuM-GC synapses (Figure 2B) (EPSC: 23.5 ± 4.6% of baseline, $n = 5$, $p < 0.001$, paired t test; IPSC: 23.9 ± 1.9% of baseline, $n = 6$, $p < 0.05$, Wilcoxon signed-rank test; EPSC vs IPSC: $p = 0.92$, unpaired t test), suggesting that both glutamate and GABA release rely on P/Q-type Ca^{2+} channels at SuM-GC synapses.

If the synaptic vesicle pools for glutamate and GABA are identical, the effects of presynaptic G-protein-coupled receptor (GPCR) modulation on both transmissions are expected to be the same. We therefore examined how glutamate/GABA co-transmission is regulated by presynaptic GPCRs. We previously demonstrated that the co-transmission of glutamate and GABA at SuM-GC synapses is presynaptically suppressed by group II metabotropic glutamate receptors (mGluRs) and $GABA_B$ receptors (Hashimotodani et al., 2018). In agreement with this, application of the group II mGluR agonist DCG-IV suppressed both EPSCs and IPSCs at SuM-GC synapses (Figure 2C). Notably, DCG-IV inhibited EPSCs ($IC_{50} = 0.11$ μM) to a greater extent than it did IPSCs ($IC_{50} = 0.27$ μM) (Figure 2C) (two-way ANOVA, $F_{1,51} = 8.1$, $p < 0.01$). Similar results were found with the application of 5 μM $GABA_B$ receptor agonist baclofen, which suppressed EPSCs more than IPSCs (Figure 2D) (EPSC: 51.6 ± 2.4% inhibition, $n = 8$; IPSC: 38.6 ± 4.3% inhibition, $n = 8$, $p < 0.05$, unpaired t test). These differential inhibitory effects of GPCRs on glutamatergic and GABAergic co-transmission are contrary to the expected idea of identical vesicle pools for glutamate and GABA but favor the hypothesis of separate vesicles for glutamate and GABA.

Spatial coupling between presynaptic Ca^{2+} channels and Ca^{2+} sensors of exocytosis is an essential feature in determining the properties of neurotransmitter release, and tight or loose coupling is distinguished by using two different binding rate Ca^{2+} chelators BAPTA and EGTA (Adler et al., 1991; Eggermann et al., 2011). We examined the effects of these two Ca^{2+} chelators on the co-transmission of glutamate and GABA. We found that the bath application of BAPTA-AM suppressed both EPSCs and IPSCs to the same extent (EPSC: 63.4 ± 12.2% of baseline, $n = 7$, $p < 0.01$, paired t test; IPSC: 63.4 ± 7.8% of baseline, $n = 8$, $p < 0.001$, paired t test; EPSC vs. IPSC: $p = 0.96$, unpaired t test) (Figure 2E). In contrast, EGTA-AM suppressed EPSCs, whereas it did not affect IPSCs (EPSC: 67.4 ± 7.2% of baseline, $n = 6$, $p < 0.01$, paired t test; IPSC: 93.1 ± 9.2% of baseline, $n = 6$, $p = 0.40$, Wilcoxon signed rank test; EPSC vs. IPSC: $p < 0.05$, unpaired t test) (Figure 2E). These results indicate tighter coupling between Ca^{2+} channels and synaptic vesicles for GABA release than for glutamate release.

Minimal light stimulation of SuM inputs elicits independent EPSCs and IPSCs in GCs

We next performed minimal light stimulation to evoke a synaptic response mediated by a single vesicle release, which allowed us to detect stochastic synaptic responses of independent EPSCs and IPSCs, or compound EPSC/IPSC responses (Kim et al., 2022). In this experiment, optical stimulation was delivered in the presence of tetrodotoxin (TTX) and 4-aminopyridine (4-AP) to exclude SuM inputs-mediated polysynaptic responses, together with D-AP5 to block NMDA receptors. We also decreased the extracellular Ca^{2+} concentration to 1 mM to reduce the release probability. At intermediate holding membrane potentials (-20 to -30 mV), maximum light power illumination elicited biphasic responses (EPSC-IPSC sequence), enabling simultaneous recordings of glutamate/GABA co-transmission in GCs (Figure 3A, left). After confirming the existence of biphasic PSCs, the light power intensity was decreased to detect small synaptic events, that were stochastically observed among the 100 times stimulations (success rate = ~15%) (Figures 3A, 3B, and Supplementary Figure 3). Using this method, we analyzed 1700 trials from 17 cells and detected 86 EPSC-only, 67 IPSC-only, and 19 biphasic events (Figures 3B and 3C). These results indicate that independent EPSCs and IPSCs are the majority of synaptic responses (Figure 3D) (EPSC: 5.1 ± 0.5% probability; IPSC: 3.9 ± 0.4% probability; biphasic: 1.1 ± 0.3% probability, $n = 17$, EPSC vs bi, $p < 0.001$; IPSC vs bi, $p < 0.001$, one-way ANOVA with Tukey's *post hoc* test). To exclude the possibility that the independent EPSCs and IPSCs detected by minimal light stimulation might have masked the putative tiny synaptic responses of their counterpart currents mediated by the associated transmitters, the amplitudes and kinetics of minimal stimulation-evoked EPSCs and IPSCs were compared with or without blockers of their counterpart receptors. We found that the amplitudes and decay of minimal light stimulation-evoked EPSCs were not changed by the application of the $GABA_A$ receptor blocker picrotoxin (Supplementary Figure 4). Similarly, the amplitudes and rise time of minimal light stimulation-evoked IPSCs were not altered by application of the AMPA/kainate receptor blocker NBQX (Supplementary Figure 4). These results validate that EPSCs and IPSCs evoked by minimal optical stimulation are mediated by the stochastic release of glutamate and GABA, respectively, from single vesicles. Furthermore, by comparing minimal stimulation-evoked PSCs with strontium-induced asynchronous PSCs (see below), we found that the amplitudes of EPSCs and IPSCs evoked by minimal stimulation were identical to those of strontium-induced asynchronous EPSCs and IPSCs, respectively (Figure 3G), suggesting that PSCs evoked by minimal stimulation were mediated by a single vesicle release.

Taken together, these results indicate that glutamatergic and GABAergic co-transmission occurs independently at SuM-GC synapses.

Asynchronous release from SuM terminals exhibits independent EPSCs and IPSCs in GCs

It should be noted that minimal light stimulation of SuM inputs may elicit synchronized release of glutamate and GABA from different vesicle pools occasionally, possibly due to synchronized opening of several Ca^{2+} channels, which could be attributed to the substantial biphasic responses we detected (Figure 3D). To minimize this possibility, we recorded asynchronous quantal PSCs by substitution of extracellular Ca^{2+} with Sr^{2+}. At intermediate holding membrane potentials (-20 to -30 mV), light pulses elicited synchronized biphasic responses in the extracellular Ca^{2+} (Figure 3E). By replacing extracellular Ca^{2+} with Sr^{2+}, asynchronous quantal synaptic responses were recorded following light stimulation of the SuM inputs (Figure 3E). By repeating the light stimulation of the SuM inputs 30 times (every 10 sec), we found that the majority of asynchronous synaptic events were EPSC-only or IPSC-only, whereas biphasic PSCs represented only a minor population (Figures 3F) (EPSC: 27.9 ± 4.7 events; IPSC: 23.4 ± 4.2 events; biphasic: 2.5 ± 0.5 events, $n = 11$, EPSC vs bi, $p < 0.001$; IPSC vs bi, $p < 0.001$, one-way ANOVA with Tukey's *post hoc* test). These results further support our conclusion that glutamate/GABA co-transmission is mediated by glutamate and GABA co-released from different populations of synaptic vesicles.

Segregated glutamatergic and GABAergic postsynaptic sites at SuM-GC synapses

We then investigated whether SuM-GC synapses exhibit distinct postsynaptic sites for each neurotransmitter using immunohistochemistry. To enhance spatial resolution, we used ultrathin sections (100 nm-thick) for analysis. As shown previously (Uchigashima et al., 2011), double immunofluorescence revealed that almost all VGluT2-positive SuM terminals in the GC layer co-expressed VIAAT (Figures 4A and 4B). Further post-embedding immunogold EM (Figures 4C and 4D) showed that these terminals formed asymmetric synapse (putative excitatory) (Figure 4C) and symmetric (putative inhibitory) synapse (Figure 4D), confirming previous observations (Boulland et al., 2009; Soussi et al., 2010; Root et al., 2018). We next applied triple immunofluorescence to detect SuM terminals by VGluT2, glutamatergic postsynaptic sites by the NMDA receptor subunit GluN1, and GABAergic postsynaptic sites by the $GABA_A$ receptor subunit $GABA_A\alpha1$. In the GC layer, almost all VGluT2-positive SuM terminals were associated with GluN1 and/or $GABA_A\alpha1$ (Figures 4E and 4F). Specifically, the majority of VGluT2-positive SuM terminals were associated with both GluN1 and $GABA_A\alpha1$ (52.5%), and the remainder were associated with $GABA_A\alpha1$ (22.1%) alone or GluN1 (25.4%) alone (Figure 4G). To investigate the spatial relationship between glutamatergic and GABAergic

250 synapses formed by individual SuM boutons, we quantified the distance between GluN1 and
251 $GABA_A\alpha1$ cluster adjacent to the same VGluT2-positive SuM bouton. On average, the
252 distance was 397.5 ± 8.75 nm and most SuM bouton (79.2%, 191 out of 241) form
253 glutamatergic and GABAergic synapse within 500 nm (Figure 4H). Taken together, these
254 results suggest that a single SuM bouton forms GluN1-containing excitatory synapse and
255 GABAAα1-containing inhibitory synapse in separate locations, yet they remain closely
256 proximal.
257
258 **Glutamate/GABA co-transmission balance of SuM inputs is dynamically changed in a**
259 **frequency-dependent manner**
260 The results described thus far indicate that the co-transmission of glutamate and GABA is
261 spatially segregated at SuM-GC synapses, thereby making it possible to independently regulate
262 the co-release of glutamate and GABA from the same SuM terminals. Due to the different
263 release properties of glutamate and GABA in the SuM terminals, glutamate/GABA co-
264 transmission could exhibit different patterns of short-term plasticity at SuM-GC synapses. To
265 test this possibility, we delivered a train of 10 light stimuli at 5-20 Hz, physiologically relevant
266 frequencies (Kirk and McNaughton, 1991; Kocsis and Vertes, 1994; Ito et al., 2018; Farrell et
267 al., 2021), to ChR2-expressing SuM inputs, and compared the short-term depression of EPSCs
268 with that of IPSCs (Figure 5A). To exclude the putative involvement of pre- and/or postsynaptic
269 modulations by mGluRs and $GABA_B$ receptors during a train of stimulation,
270 pharmacologically isolated EPSCs or IPSCs were recorded in the presence of the broad-
271 spectrum mGluR antagonist LY341495 (100 μM) and $GABA_B$ receptor antagonist CGP55845
272 (3 μM). We found that trains of 10 light stimuli at 5, 10, and 20 Hz elicited pronounced short-
273 term synaptic depression of EPSCs during train with stronger depression at higher frequencies
274 (Figures 5A and 5B). We further performed the same experiments under recording conditions
275 with a low release probability by reducing the extracellular Ca^{2+} concentration from 2.5 to 1
276 mM. While train stimulation elicited a weaker depression than 2.5 mM extracellular Ca^{2+},
277 frequency-dependent depression was still observed (Figure 5C). In marked contrast to EPSCs,
278 while IPSCs also exhibited short-term synaptic depression across all tested frequencies,
279 GABAergic co-transmission showed a similar magnitude of depression across all frequencies
280 (Figures 5D and 5E). Similarly, short-term depression of IPSCs did not show a frequency-
281 dependent depression with 1 mM extracellular Ca^{2+} (Figure 5F), leading to a sustained
282 inhibitory effect at any frequency. Given that EPSCs show strong frequency-dependent
283 depression, whereas IPSCs exhibit frequency-independent sustained depression, it is likely that

284 the EPSC/IPSC ratio can decrease during high-frequency train stimulation. Indeed, comparing
285 the amplitudes of the 10th EPSCs with those of the 10th IPSCs indicated that the depression of
286 EPSCs was stronger than that of IPSCs at 10 Hz and 20 Hz (Figure 5G). We further addressed
287 whether short-term dynamic changes in the EPSC/IPSC ratio could be observed in the same
288 cell by recording the biphasic synaptic responses at intermediate membrane potentials that
289 enabled simultaneous monitoring of the compound EPSC/IPSC. We found that 10 Hz train
290 light illumination induced a stronger depression of EPSCs than of IPSCs (Supplementary
291 Figures 5A and 5B), thereby decreasing the EPSC/IPSC ratio during the high-frequency train
292 stimulation.

293 Despite the differential properties of the co-release of glutamate and GABA from SuM
294 terminals, the difference in the magnitude of short-term depression between glutamatergic and
295 GABAergic co-transmission could be mediated by postsynaptic mechanisms, such as AMPA
296 receptor saturation and desensitization during burst high-frequency stimulation (Trussell et al.,
297 1993; Brenowitz and Trussell, 2001; Heine et al., 2008). To test this possibility, we recorded
298 EPSC trains in the presence of γ-D-glutamylglycine (γDGG), a low-affinity AMPA receptor
299 antagonist that relieves AMPA receptor saturation and desensitization (Wadiche and Jahr, 2001;
300 Wong et al., 2003; Foster and Regehr, 2004). As expected, 2 mM γDGG reduced the amplitude
301 of EPSCs (60.1 ± 4.3% reduction, $n = 16$, $p < 0.001$, paired t test). Under these conditions,
302 short-term depression with high-frequency light stimulation (10 Hz and 20 Hz) was not
303 affected (Supplementary Figures 6A and 6B), excluding the postsynaptic contribution to the
304 strong depression of EPSCs, suggesting that the short-term depression of EPSCs is mediated
305 by presynaptic mechanisms. Similarly, to determine whether postsynaptic $GABA_A$ receptor
306 saturation is involved in short-term depression during train stimulation, we used the low-
307 affinity competitive $GABA_A$ receptor antagonist TPMPA (Sakaba, 2008; Markwardt et al.,
308 2009; Turecek et al., 2016). We found that 300 μM TPMPA reduced the amplitude of IPSCs
309 (47.1 ± 3.8% reduction, $n = 11$, $p < 0.01$, Wilcoxon signed rank test), while short-term
310 depression of IPSCs in response to 10 light pulses at 10 Hz and 20 Hz did not differ before and
311 after the application of TPMPA (Supplementary Figures 6C and 6D), excluding the
312 involvement of $GABA_A$ receptor saturation in the short-term depression of IPSCs at SuM-GC
313 synapses, suggesting a presynaptic origin of this short-term plasticity.

314 Taken together, these results suggest that SuM-GC synapses exhibit short-term dynamic
315 changes in the glutamate/GABA co-transmission ratio during repetitive high-frequency SuM
316 activity due to the different properties of frequency-dependent depression between
317 glutamatergic and GABAergic transmission, favoring inhibition over excitation. Furthermore,

the different properties of short-term depression of EPSCs and IPSCs also support the segregated co-transmission of glutamate and GABA at SuM-GC synapses.

SuM inputs modulate GC activity in a frequency dependent manner

We have previously demonstrated that SuM inputs associated with entorhinal cortex (EC) inputs facilitate GC firing (Hashimotodani et al., 2018). Our previous study investigated the single association of synaptic inputs, but did not examine repetitive stimulation of synaptic inputs. We investigated how the repetitive activation of SuM inputs, which implement frequency-dependent filtering of glutamatergic responses with sustained synaptic inhibition by GABAergic co-transmission, affects GC excitability. To mimic excitatory EC synaptic inputs onto GCs, a sinusoidal current was injected into the soma of GCs (Kamondi et al., 1998; Magee, 2001; Ajibola et al., 2021), which can bypass direct synaptic stimulation of the performant path (main excitatory inputs originating from EC) and, consequently, circumvent the recruitment of inhibitory circuitry. We found that a sinusoidal current at 5 Hz generated action potentials at the peak of the depolarizing phase (Figure 6A). The injected current was adjusted to generate action potentials with fewer than five spikes in each trial (10 cycles), and the optogenetically activated SuM inputs were paired at the depolarizing phase of each cycle. Paired light illumination significantly enhanced GC firing compared to sinusoidal current injections without light stimulation throughout the trial (10 stimuli) (Figures 6A and 6D). Notably, the probability of spikes further increased when GABAergic transmission was blocked by picrotoxin (Figures 6A and 6D). These results suggest that SuM inputs enhance GC firing and that GABAergic co-transmission negatively regulates the net excitatory effect of SuM inputs at 5 Hz, similar to the effects of a single associational activation of SuM and EC inputs (Hashimotodani et al., 2018). In striking contrast, at higher frequencies (10 Hz and 20 Hz), the enhancement of spike probability by SuM activation was attenuated and disappeared in the last few stimulations (Figures 6B, 6C, 6E, and 6F). Importantly, in the presence of picrotoxin, SuM activation by light stimulation enhanced GC firing, even in the last few stimulations (Figures 6B, 6C, and 6E, 6F), suggesting that SuM glutamatergic co-transmission still exerted excitatory effects in the later cycle, even during the short-term depression of glutamate release. Thus, the excitatory action of SuM inputs was filtered by the co-released GABA during repetitive high-frequency stimulation due to frequency-independent sustained depression. These results indicate that SuM inputs modulate GC output in a frequency-dependent manner due to the different short-term plasticities of glutamate/GABA co-transmission.

352 **Discussion**

353 Despite evidence that glutamate and GABA are co-released from the synaptic terminals of a
354 subset of neurons in the adult brain, whether glutamate and GABA are released from the same
355 or distinct synaptic vesicle populations remains a debate (Shabel et al., 2014; Root et al., 2018;
356 Kim et al., 2022). In this study, we demonstrate that the transmission properties of glutamate
357 and GABA at SuM-GC synapses differ in PPR, Ca^{2+}-sensitivity, presynaptic GPCR regulation,
358 and Ca^{2+} channel-synaptic vesicle coupling configuration. We further found that uniquantal
359 synaptic responses exhibit independent EPSCs and IPSCs. The anatomical results show that
360 the postsynaptic excitatory site (labeled by GluN1) and inhibitory site (labeled by $GABA_A\alpha1$)
361 facing the same SuM terminals are separated with close distance. These findings provide
362 evidence that glutamatergic and GABAergic co-transmission occurs at functionally distinct
363 release sites (Figure 7). Owing to the functional and spatial segregation of the co-transmission
364 of glutamate and GABA, each transmission exhibits distinct short-term plasticities, leading to
365 different frequency-dependent effects of SuM inputs on the GC activity.

366 Different release properties of dual-neurotransmitter neurons have been reported in other
367 synaptic circuits. Different PPRs (Lee et al., 2010; Silm et al., 2019; Zych and Ford, 2022) and
368 Ca^{2+}-sensitivities (Lee et al., 2010; Zych and Ford, 2022) between co-transmission of dual-
369 neurotransmitters are found in the retina (acetylcholine and GABA) and striatum (dopamine
370 and glutamate or GABA). Different reliance on Ca^{2+} channels for distinct neurotransmitters
371 have been reported in the retina (acetylcholine and GABA) (Lee et al., 2010), striatum
372 (dopamine and glutamate) (Silm et al., 2019), and hippocampus (acetylcholine and GABA)
373 (Takacs et al., 2018). These different release properties of the two neurotransmitters indicate a
374 separate release from distinct vesicle pools (Lee et al., 2010; Takacs et al., 2018; Silm et al.,
375 2019). Our study also demonstrated that glutamate and GABA co-release from SuM terminals
376 shows differences in PPR and Ca^{2+}-sensitivity. Glutamatergic transmission exhibited a stronger
377 depression than GABAergic transmission, suggesting that release probability of glutamate is
378 higher than that of GABA. A higher reduction in IPSCs than EPSCs by decreasing the
379 extracellular Ca^{2+} concentration from 2.5 to 1 mM indicates that GABA release requires higher
380 extracellular Ca^{2+} than glutamate release. Furthermore, using the Ca^{2+} chelators BAPTA and
381 EGTA, we found that the spatial coupling between Ca^{2+} channels and synaptic vesicles of
382 GABA is tighter than that of glutamate. These differences in release properties can be attributed
383 to the different compositions of the release machinery and different spatial organizations
384 between the release machinery and Ca^{2+} channels for glutamate and GABA release (Sudhof,
385 2013; Neher and Brose, 2018). Given that GABAergic co-transmission exhibits a lower release

386 probability and a higher requirement for extracellular Ca^{2+}, together with tight coupling
387 between Ca^{2+} channels and vesicles, synaptic vesicles for GABA release could be surrounded
388 by a few Ca^{2+} channels in close proximity. In contrast, the synaptic vesicles for glutamate
389 release could be surrounded by a large number of Ca^{2+} channels at longer distances than those
390 for GABA release. As other possible mechanisms, the molecular identity and composition of
391 the release machinery may differ between glutamate and GABA release. Future studies will
392 have to investigate the differences in the release machinery of glutamate and GABA.

393 Our data showed that both glutamate and GABA release rely on P/Q-type Ca^{2+} channels at
394 SuM-GC synapses. Interestingly, the excitatory transmission of SuM-CA2 pyramidal neuron
395 synapses, an exclusive glutamatergic synapse (Chen et al., 2020), is also mediated by P/Q-type
396 Ca^{2+} channels (Robert et al., 2021). Therefore, neurotransmitter release from SuM neurons
397 depends on P/Q-type Ca^{2+} channels, irrespective of the target neurons. We found that the
398 activation of group II mGluRs and $GABA_B$ receptors inhibited glutamatergic co-transmission
399 more strongly than GABAergic co-transmission. Given that these GPCRs suppress presynaptic
400 Ca^{2+} channels via $G_{i/o}$-protein, and that both transmitter releases are mediated by the same type
401 of Ca^{2+} channels, the different extents of inhibition of the co-release of glutamate/GABA by
402 group II mGluRs and $GABA_B$ receptors may be attributed to differential expression levels of
403 receptors or signaling efficacy between glutamate and GABA release.

404 A previous EM studies reported that a single SuM terminal forms symmetric and
405 asymmetric synapses in the DG (Boulland et al., 2009; Soussi et al., 2010; Root et al., 2018;
406 Billwiller et al., 2020). However, confirming whether these synapses function as glutamatergic
407 or GABAergic relies on the identification of their postsynaptic receptors, which remains
408 unresolved. In our study, we demonstrated that both GluN1 and $GABA_A\alpha1$ were associated
409 with common SuM boutons (Figures 4E and 4F), suggesting that these synapses represent
410 distinct glutamatergic and GABAergic synapses. Furthermore, our analysis showed that
411 approximately 50% of SuM boutons was associated with both GluN1 and $GABA_A\alpha1$ (Figure
412 4G). It should be noted, however, this percentage can be an underestimate due to the utilization
413 of 100 nm-thick ultrathin sections, which limits the detection of co-localization events within
414 this confined spatial range. Consequently, the actual percentage is expected to be significantly
415 higher. Hence, the predominant synapse type of SuM boutons consists of dual glutamatergic
416 and GABAergic synapses, with additional individual glutamatergic or GABAergic synapses.

417 Previous electrophysiological studies have demonstrated that both glutamate and GABA
418 are co-packaged in the same synaptic vesicles in the lateral habenula (Shabel et al., 2014; Kim
419 et al., 2022). Minimal optogenetic stimulation of EP terminals evoked a high proportion of

420 biphasic PSCs over independent EPSCs and IPSCs in lateral habenular neurons, suggesting the
421 co-release of glutamate and GABA from the same synaptic vesicles (Kim et al., 2022). While
422 these findings seem to be contradictory with anatomical data showing distinct populations of
423 synaptic vesicles for glutamate and GABA in the lateral habenula (Root et al., 2018), there
424 could be technical limitations for immuno EM to examine the spatial distributions of proteins
425 in the vesicles (Kim and Sabatini, 2023), such as interference of antibodies with each other on
426 a tiny vesicle, limitations of antibody access to target molecules, and the stochastic nature of
427 labeling two molecules in a single vesicle. In addition, the existence of VTA terminals, other
428 glutamate/GABA co-release inputs (Root et al., 2014; Yoo et al., 2016; Root et al., 2018), may
429 complicate interpretation of the co-release mechanisms in the lateral habenula. In contrast, in
430 the DG, we found that the majority of synaptic responses evoked by both minimal light
431 stimulation and asynchronous release at SuM-GC synapses showed independent EPSCs and
432 IPSCs. A previous biochemical study detected VGluT2 and VIAAT in distinct purified synaptic
433 vesicles from the hippocampus (Boulland et al., 2009). Moreover, differences in transport
434 mechanisms between glutamatergic and GABAergic vesicles have been reported (Farsi et al.,
435 2016). Based on this evidence, our results most likely support the hypothesis that glutamate
436 and GABA are packaged in distinct synaptic vesicles (Figure 7). Thus, glutamate/GABA co-
437 transmission is diverse, in that both transmitters are co-released from the same or different
438 synaptic vesicles, depending on brain regions and synapse types.

439 The distinct co-transmission modes of the two transmitters have the ability to exert
440 independent synaptic regulation compared with their co-release from identical vesicles. At
441 SuM-GC synapses, we demonstrated that glutamatergic and GABAergic co-transmission
442 exhibited different short-term plasticities. While glutamatergic co-transmission showed strong
443 frequency-dependent depression, GABAergic co-transmission exhibited stable frequency-
444 independent depression. By this frequency-specific dynamic change of the glutamate/GABA
445 co-transmission balance, at low-frequency burst SuM inputs, they operated as excitatory inputs,
446 whereas at high frequency, the excitatory effects of SuM inputs on GCs were inhibited by co-
447 transmitted GABA (Figure 6). Accordingly, GCs respond differently to SuM inputs in a
448 frequency-dependent manner, due to the low-pass filtering of SuM-GC synapses. The fact that
449 the theta-rhythm in the hippocampus is associated with synchronized SuM activity (Kirk and
450 McNaughton, 1991; Kocsis and Vertes, 1994; Ito et al., 2018; Farrell et al., 2021) has important
451 implications for the low-pass filtering of this synapse. As SuM inputs act as excitatory at 5 Hz
452 (theta) train stimulation, but not at higher frequencies, SuM inputs may transfer their train
453 information exclusively at the theta frequency, which could contribute to theta-mediated

information processing in SuM-hippocampal circuits and their relevant brain functions, including cognitive, sleep, and navigation processes (Pedersen et al., 2017; Billwiller et al., 2020; Chen et al., 2020; Li et al., 2020; Farrell et al., 2021; Kesner et al., 2023). In addition to SuM inputs, GCs receive EC inputs as the main excitatory inputs for discharge, and other excitatory inputs from hilar mossy cells (Hashimotodani et al., 2017). Therefore, low-pass filtering of SuM inputs could prevent the over-excitation of GCs, leading to anti-seizure effects. In contrast to the presynaptic origin of short-term plasticity at SuM-GC synapses, we previously demonstrated the postsynaptically induced long-term potentiation at SuM-GC synapses, which selectively occurs of glutamatergic co-transmission (Hirai et al., 2022; Tabuchi et al., 2022). Our findings suggest that SuM inputs play diverse roles in modulating GC output via short- and long-term plasticity with pre- and postsynaptic distinct mechanisms, respectively.

Materials and Methods

Animals

C57BL/6 and VGluT2-Cre mice (Jackson Labs, Slc17a6$^{tm2(cre)Lowl}$/J, stock #016963) of either sex aged 6-7 weeks were used for electrophysiological experiments and male C57BL/6 mice at 2–3 months of age were used for anatomical experiments (Figure 4). All animals were group housed in a temperature- and humidity-controlled room under a 12 hr light/12 hr dark cycle. Water and food were provided *ad libitum*. The experiments were approved by the animal care and use committee of Doshisha University and Hokkaido University and were performed in accordance with the guidelines of the committees.

Stereotaxic viral injections

Mice on postnatal days 19 to 21 were placed in a stereotaxic frame, and anesthetized with isoflurane (1.5–2.5%). A beveled glass capillary pipette connected to a microsyringe pump (UMP3, WPI) was used for the viral injection. 200 nL of AAV1-EF1a-DIO-hChR2(H134R)-eYFP (Addgene) was injected into the SuM (relative to bregma, AP: −2.2 mm, ML: ±0.5 mm, DV: −4.85 mm) at a rate of 50 nL/min. The glass capillary was remained at the target site for 5 min before the beginning of the injection and was removed 10 min after infusion.

Hippocampal slice preparation

Acute transverse hippocampal slices (300 μm thick) were prepared from mice 3–4 weeks after AAV injection. The mice were decapitated under isoflurane anesthesia. Briefly, the hippocampi were isolated, embedded in an agar block, and cut using a vibratome (VT1200S, Leica Microsystems) in an ice-cold cutting solution containing (in mM): 215 sucrose, 20 D-glucose, 2.5 KCl, 26 $NaHCO_3$, 1.6 NaH_2PO_4, 1 $CaCl_2$, 4 $MgCl_2$, and 4 $MgSO_4$. Brain blocks, including the interbrain and midbrain, were also isolated and fixed in 4% paraformaldehyde (PFA) for *post hoc* our internal check of the injection site (Tabuchi et al., 2022). Hippocampal slices were transferred to an incubation chamber and incubated at 33.5°C in the cutting solution. After 30 min of incubation, the cutting solution was replaced with an extracellular artificial cerebrospinal fluid (ACSF) containing (in mM): 124 NaCl, 2.5 KCl, 26 $NaHCO_3$, 1 NaH_2PO_4, 2.5 $CaCl_2$, 1.3 $MgSO_4$ and 10 D-glucose at 33.5°C. The slices were stored at room temperature for at least 1 h before recording. Both the cutting solution and the ACSF were oxygenated with 95% O_2 and 5% CO_2. After recovery, slices were transferred to a submersion-type recording chamber for electrophysiological analysis.

Electrophysiology

Whole-cell recordings using an EPC10 (HEKA Electronik) or IPA amplifier (Sutter Instruments) were made from GCs using an infrared differential interference contrast microscopy (IR-DIC, Olympus, BX51WI). We recorded from GCs with an input resistance of < 300 MΩ for mature GCs (Schmidt-Hieber et al., 2004). The data were filtered at 2.9 kHz and sampled at 20 kHz. For voltage-clamp recordings, we used patch pipettes (3–6 MΩ) filled with an intracellular solution with the following composition (in mM): 131 Cs-gluconate, 4 CsCl, 10 HEPES, 0.2 EGTA, 2 Mg-ATP, 0.3 Na_3GTP, 10 phosphocreatine, pH 7.3 adjusted with CsOH (the calculated E_{Cl-} = –90 mV) (292-300 mOsm). For recordings of synaptic currents at intermediate membrane potentials, 5 mM QX314 was included in the intracellular solution. ChR2-expresing SuM fibers were activated at 0.05 Hz by a pulse of 470 nm blue light (1-5 ms duration, 5.0-10.5 mW/mm^2) delivered through a 40× objective attached to a microscope using an LED (Mightex or ThorLabs). The light intensity was adjusted to yield less than 80% of the maximum response during the baseline period. The illumination field was centered over the recorded cell, unless otherwise stated. Series resistance (8–20 MΩ) was uncompensated and monitored throughout experiments with a –5 mV, 50 ms voltage step, and cells that exhibited a significant change in the series resistance more than 20% were excluded from analysis.

For minimal light stimulation experiments, we first recorded biphasic synaptic responses from GCs by maximum light stimulation of SuM inputs at intermediate membrane potentials

522 from -20 to -30 mV in the presence of 1 μM TTX, 1 mM 4-AP, 50 μM D-AP5, and 1 mM Ca^{2+}.
523 The exact membrane potentials were set to the potential at which the amplitudes of EPSCs and
524 IPSCs were similar. Then, light power intensity was decreased to detect small stochastic
525 synaptic events. We adjusted the light power (<1 ms duration, <1.0 mW/mm^2) to evoke
526 synaptic responses, with a success rate of 15%. A total of 100 trials were recorded every 10 s.
527 EPSC-only responses were determined as the synaptic current with the onset of a downward
528 deflection within 6 ms of light illumination that returned to the baseline without an outward
529 current within 20 ms of light illumination. IPSC-only responses were determined as the
530 synaptic current with the onset of an upward deflection within 6 ms of light illumination,
531 without an inward current immediately after light illumination. Biphasic responses were
532 defined as an EPSC-IPSC sequence, only if an outward peak current following an inward
533 current appeared within 20 ms of light illumination. The amplitude threshold was set to three
534 times the SD of the baseline noise. Based on these criteria, we confirmed that the detection rate
535 of false-positive events (without light illumination) was 0.6 ± 0.4% (3/500 trials, n = 5).
536 For recordings of asynchronous synaptic events, we initially recorded light stimulation-
537 evoked biphasic synaptic responses at intermediate membrane potentials (-20 to -30 mV) in
538 the presence of Ca^{2+}. The ACSF was then replaced with Ca^{2+}-free ACSF containing 4 mM
539 $SrCl_2$. Asynchronous synaptic responses were evoked by light pulses at 0.1 Hz for 30 times,
540 measured during a 450 ms period beginning 30 ms after the stimulus to exclude the initial
541 synchronous synaptic responses, and analyzed using the Mini Analysis Program (Synaptosoft).
542 D-AP5 (50 μM) was included in the extracellular ACSF throughout the experiment to eliminate
543 NMDA receptor-mediated currents.
544 For train stimulation, EPSCs were recorded from GCs at a holding potential of -70 mV in
545 the presence of 100 μM picrotoxin, while IPSCs were recorded at a holding potential of 0 mV
546 in the presence of 10 μM NBQX and 50 μM D-AP5. Biphasic PSCs were recorded at a holding
547 potential of -30 mV in the presence of 1 μM TTX, 500 μM 4-AP, and 50 μM D-AP5. In all
548 train-stimulation experiments, 100 μM LY341495 and 3 μM CGP55845 were also added to the
549 ACSF throughout the experiments. 10 light pulses at 5 Hz, 10 Hz, and 20 Hz were delivered
550 every 20 sec, and 10–20 sweeps were recorded.
551 For field potential recordings in the CA1 region, a recording pipette filled with 1 M NaCl
552 and a patch pipette with broken tip (with diameter of ~20–30 μm) filled with the ACSF were
553 placed in the stratum radiatum of the CA1 region.
554 For current-clamp recordings, we used an intracellular solution with the following
555 composition (in mM): 135 $KMeSO_4$, 5 KCl, 10 HEPES, 0.2 EGTA, 2 MgATP, 0.3 Na_3GTP, 10

556 phosphocreatine, pH 7.3 adjusted with NaOH (the calculated E_{Cl-} = −82 mV) (297−299 mOsm).
557 A sinusoidal current was delivered to the soma of GCs at 5 Hz, 10 Hz, and 20 Hz (10 cycles),
558 while the membrane potential was held at -70 mV to -80 mV. The injected current (100−240
559 pA) was adjusted to generate action potentials with fewer than five spikes in each trial. After
560 obtaining control, a sinusoidal current injection was paired with light stimulation of SuM inputs
561 at the depolarizing phase of each cycle. Subsequently, 100 μM picrotoxin was bath applied,
562 and the same pairing of sinusoidal current with light stimulation were delivered. In each
563 experiment, 10 trials were recorded every 20 sec.
564 All experiments were performed at 30−33°C in the recording chamber perfused (2
565 mL/min) with oxygenated ACSF.
566
567 **Pharmacology**
568 Each reagent was dissolved in water, NaOH or DMSO, depending on the manufacture's
569 recommendation to prepare a stock solution, and stored at −20°C. NBQX, D-AP5, (RS)-
570 baclofen, DCG-IV, γDGG, TPMPA, and LY341495 were purchased from Tocris Bioscience.
571 ω−Conotoxin GVIA and ω−agatoxin IVA were purchased from the Peptide Institute. Picrotoxin
572 was purchased from the Tokyo Chemical Industry. 4-AP and BAPTA-AM were purchased from
573 nacalai tesque. TTX was purchased from Fujifilm Wako Pure Chemical. EGTA-AM was
574 purchased from AAT Bioquest. CGP55845 was purchased from Hello Bio. Reagents were bath
575 applied following dilution into ACSF from the stock solutions immediately before use.
576
577 **Antibodies**
578 Primary antibodies raised against the following molecules were used: $GABA_A$ receptor γ2
579 subunit, NMDA receptor GluN1 subunit, VGluT2, VIAAT, and GFP. Information on the
580 molecule, antigen sequence, host species, specificity, reference, NCBI GenBank accession
581 number, and RRID of the primary antibodies used is summarized in Table S1.
582
583 **Immunohistochemistry for ChR2-expressing SuM terminals**
584 Under deep pentobarbital anesthesia (100 mg/kg of body weight, intraperitoneally), AAV-DIO-
585 ChR2(H134R)-eYFP injected VGluT2-Cre mice were perfused with 4% PFA. Brains were
586 removed and stored in 4% PFA for 4 h at room temperature, then transferred to PBS and left
587 overnight at 4°C. Coronal brain slices containing the SuM or the hippocampus were sectioned
588 at 100 μm using a vibratome (VT1200S, Leica microsystems). After permeabilization in PBS
589 with 1% Triton X-100 for 30 min, the sections were blocked in PBS with 5% donkey serum

590 for 1h. After washing three times with PBS for 10 min each, the sections were incubated in
591 PBS containing primary antibodies and 0.5% Triton X-100 overnight at room temperature.
592 Primary antibodies against GFP (goat, 1:200), VGluT2 (rabbit, 1:200), and VIAAT (guinea pig,
593 1:200) were used. The sections were then rinsed with PBS three times, and incubated in PBS
594 containing 0.5% Triton X-100 and secondary donkey antibodies (1:500, anti-goat Alexa Fluor
595 488-conjugated antibody, abcam, ab150129; anti-rabbit Alexa Fluor 568-conjugated antibody,
596 abcam, ab175470; anti-guinea pig Cy5-conjugated antibody, Jackson ImmunoResearch, 706-
597 175-148) for 2h at room temperature. Sections were rinsed three times in PBS and mounted on
598 glass slides with DAPI. To analyze colocalization of ChR2-eYFP-labeled axonal boutons with
599 VGluT2 and VIAAT, z stack images were captured (0.4 μm optical sections) using a
600 fluorescence microscope (BZ-X800, Keyence). Swellings of ChR2-YFP labeled axons were
601 considered as axonal boutons, and their colocalization with VGluT2 and VIAAT
602 immunofluorescence was examined in 3D planes as previously reported (Hashimotodani et al.,
603 2018).
604
605 **Immunofluorescence using ultrathin sections**
606 Under deep pentobarbital anesthesia (100 mg/kg body weight, i.p.), mice were fixed by
607 transcardially with 5 ml of saline, followed by 60 ml of glyoxal fixative solution (9% glyoxal
608 [Sigma], 8% acetic acid, pH 4.0) (Konno et al., 2023). Brains were dissected and post-fixed at
609 4°C in glyoxal fixative solution for 2 hr. Coronal 400-μm-thick brain sections were cut on a
610 vibratome (VT1000S, LeicaMicrosystems). Sections were embedded in durcupan (Sigma) and
611 ultra-thin sections (100 nm-thick) were prepared by Ultracut ultramicrotome (Leica
612 Microsystems). Sections were mounted on silane-coated glass slides (New Silane II, *Muto* Pure
613 Chemicals). After etching with saturated sodium ethanolate solution for 1–5 s, ultra-thin
614 sections on slides were treated with ImmunoSaver (Nisshin EM) at 95°C for 30 min. Sections
615 were blocked with 10% normal donkey serum (Jackson ImmunoResearch) for 20 min, then
616 incubated with a mixture of primary antibody solution (1 μg/ml in phosphate-buffered saline
617 (pH 7.2) containing 0.1% TritonX-100 (PBST) overnight at room temperature. Sections were
618 washed three times with PBST and incubated with a solution of Alexa488, Cy3, and Alexa647-
619 labeled species-specific secondary antibodies (Jackson ImmunoResearch; Thermo Fisher
620 Scientific) diluted at 1:200 in PBST for 2 h at room temperature. After washing, sections were
621 air-dried, and mounted with using ProLong Glass (Thermo Fisher Scientific). Photographs
622 were taken with a confocal laser microscope (FV1200, Evident) using 20x and 60x objectives.
623

624 **Postembedding immunoelectron microscopy**

625 Under deep anesthesia with pentobarbital (100 mg/kg, i.p.), mice were transcardially perfused
626 with 4% PFA/0.1 M PB (pH 7.2) for 10 min, brains were removed, postfixed for 2 h in the
627 same fixative, and coronal sections (400 μm-thick) prepared using a vibratome (VT1000S,
628 Leica Microsystems). Then, sections were cryoprotected with 30% glycerol in PB, and frozen
629 rapidly with liquid propane in the EM CPC unit (Leica Microsystems). Frozen sections were
630 immersed in 0.5% uranyl acetate in methanol at –90°C in the AFS freeze-substitution unit
631 (Leica Microsystems), infiltrated at –45°C with Lowicryl HM-20 resin (Chemische Werke
632 Lowi, Waldkraiburg, Germany), and polymerized with ultraviolet light. Ultrathin sections were
633 made using an Ultracut ultramicrotome (Leica Microsystems). Ultrathin sections (100 nm
634 thick) mounted on nickel grids were etched with ultrathin sections on nickel grids were etched
635 with saturated sodium-ethanolate solution for 1–5 s. For double labeling against VGluT2 and
636 VIAAT, sections were incubated in blocking solution containing 2% normal goat serum
637 (Nichirei, Tokyo, Japan) in 0.03% Triton X-100 in Tris-buffered saline (TBST, pH 7.4),
638 followed by VIAAT antibody (20 μg/ml) diluted in 2% normal goat serum in TBST overnight,
639 then colloidal gold-conjugated (5 nm) anti-rabbit IgG in blocking solution for 2 hr. After
640 extensive washing in distilled water, sections were incubated in blocking solution containing
641 2% rabbit serum (Nichirei, Tokyo, Japan) in TBST for 10 min, VGluT2 antibody (20 μg/ml)
642 diluted with 2% normal rabbit serum in TBST overnight, and colloidal gold-conjugated (10
643 nm) anti-guinea pig IgG in blocking solution for 2 hr. After extensive washing in distilled water,
644 sections were fixed with 2% OsO4 for 15 min, then stained with 5% uranyl acetate/40% EtOH
645 for 90 s and Reynold's lead citrate solution for 60 s. Photographs were taken from the granular
646 layer of the dentate gyrus with an H-7100 electron microscope at x20,000 magnification.

647

648 **Data analysis**

649 The PPR was defined as the ratio of the amplitude of the second PSCs to the amplitude of the
650 first PSCs (100 ms inter-stimulus interval). The reduction in PSCs by a decrease in extracellular
651 Ca^{2+} concentration was determined by comparing 10 min baseline responses (2.5 mM Ca^{2+})
652 with responses 20–25 min after replacement of extracellular Ca^{2+} (1 mM). The inhibition of
653 PSCs by DCG-IV, baclofen, ω-CgTx, ω–Aga-IVA, BAPTA-AM, and EGTA-AM was
654 determined by comparing the 10 min baseline responses with responses at 15–20 min (or 25–30
655 min for BAPTA-AM, and EGTA-AM) after each drug application. The PSCs probability was
656 calculated as the percentage of the number of synaptic responses among 100 sweeps. Train
657 stimulation-induced depression was calculated as the ratio of the amplitude of the second to

10th PSCs to the amplitude of the first PSCs. Each stimulus point had an averaged of 10–20 sweeps. Spike probability was calculated as the percentage of the number of spikes among 10 trials.

Statistics

Statistical analyses were performed using OriginPro software (OriginLab, USA). Normality of the distributions was assessed using the Shapiro–Wilk test. For samples with normal distributions, Student's unpaired and paired two-tailed t tests were used to assess the between-group and within-group differences, respectively. For samples that were not normally distributed, a non-parametric paired sample Wilcoxon signed-rank test was used. The Kolmogorov–Smirnov test was used for cumulative distributions. Differences among two or multiple samples were assessed by using one-way or two-way ANOVA followed by Tukey's *post hoc* test for multiple comparisons. Statistical significance was set at $p < 0.05$ (***, **, and * indicates $p < 0.001$, $p < 0.01$ and $p < 0.05$, respectively). All values are reported as the mean ± SEM.

Acknowledgement

This work was supported by the Grants-in-Aid for Scientific Research (24KJ2139 to H. H.; 20KK0171 and 24K02125 to T.S.; 20H03358, 23H04240, and 23K18167 to Y.H.) from Japan Society for the Promotion of Science (JSPS), the Takeda Science Foundation (to Y.H.), the Naito Foundation (to Y.H.), the Mochida Memorial Foundation for Medical and Pharmaceutical Research (to Y.H.) and JSPS Core-to-Core Program A. Advanced Research Networks (grant number: JPJSCCA20220007 to T.S.).

Author contributions

T.S. and Y.H. designed the experiments. H.H. and Y.H. performed the experiments and data analysis. K.K., M.Y. and M.W. designed and performed the immunohistochemistry experiments. Y.H. wrote the manuscript with input from all authors.

Declaration of interests

The authors declare no competing interests.

692 **References**

693

694 Adler EM, Augustine GJ, Duffy SN, Charlton MP (1991) Alien intracellular calcium chelators
695 attenuate neurotransmitter release at the squid giant synapse. J Neurosci 11:1496-1507.

696 Ajibola MI, Wu JW, Abdulmajeed WI, Lien CC (2021) Hypothalamic Glutamate/GABA
697 Cotransmission Modulates Hippocampal Circuits and Supports Long-Term
698 Potentiation. J Neurosci 41:8181-8196.

699 Billwiller F, Castillo L, Elseedy H, Ivanov AI, Scapula J, Ghestem A, Carponcy J, Libourel PA,
700 Bras H, Abdelmeguid NE, Krook-Magnuson E, Soltesz I, Bernard C, Luppi PH,
701 Esclapez M (2020) GABA-glutamate supramammillary neurons control theta and
702 gamma oscillations in the dentate gyrus during paradoxical (REM) sleep. Brain Struct
703 Funct 225:2643-2668.

704 Boulland JL, Jenstad M, Boekel AJ, Wouterlood FG, Edwards RH, Storm-Mathisen J,
705 Chaudhry FA (2009) Vesicular glutamate and GABA transporters sort to distinct sets of
706 vesicles in a population of presynaptic terminals. Cereb Cortex 19:241-248.

707 Brenowitz S, Trussell LO (2001) Minimizing synaptic depression by control of release
708 probability. J Neurosci 21:1857-1867.

709 Chen S, He L, Huang AJY, Boehringer R, Robert V, Wintzer ME, Polygalov D, Weitemier AZ,
710 Tao Y, Gu M, Middleton SJ, Namiki K, Hama H, Therreau L, Chevaleyre V, Hioki H,
711 Miyawaki A, Piskorowski RA, McHugh TJ (2020) A hypothalamic novelty signal
712 modulates hippocampal memory. Nature 586:270-274.

713 Eccles JC, Fatt P, Koketsu K (1954) Cholinergic and inhibitory synapses in a pathway from
714 motor-axon collaterals to motoneurones. J Physiol 126:524-562.

715 Eggermann E, Bucurenciu I, Goswami SP, Jonas P (2011) Nanodomain coupling between
716 Ca(2)(+) channels and sensors of exocytosis at fast mammalian synapses. Nat Rev
717 Neurosci 13:7-21.

718 Farrell JS, Lovett-Barron M, Klein PM, Sparks FT, Gschwind T, Ortiz AL, Ahanonu B,
719 Bradbury S, Terada S, Oijala M, Hwaun E, Dudok B, Szabo G, Schnitzer MJ,
720 Deisseroth K, Losonczy A, Soltesz I (2021) Supramammillary regulation of locomotion
721 and hippocampal activity. Science 374:1492-1496.

722 Farsi Z, Preobraschenski J, van den Bogaart G, Riedel D, Jahn R, Woehler A (2016) Single-
723 vesicle imaging reveals different transport mechanisms between glutamatergic and
724 GABAergic vesicles. Science 351:981-984.

725 Foster KA, Regehr WG (2004) Variance-mean analysis in the presence of a rapid antagonist
726 indicates vesicle depletion underlies depression at the climbing fiber synapse. Neuron
727 43:119-131.

728 Hashimotodani Y, Karube F, Yanagawa Y, Fujiyama F, Kano M (2018) Supramammillary
729 Nucleus Afferents to the Dentate Gyrus Co-release Glutamate and GABA and
730 Potentiate Granule Cell Output. Cell Rep 25:2704-2715 e2704.

731 Hashimotodani Y, Nasrallah K, Jensen KR, Chavez AE, Carrera D, Castillo PE (2017) LTP at
732 Hilar Mossy Cell-Dentate Granule Cell Synapses Modulates Dentate Gyrus Output by
733 Increasing Excitation/Inhibition Balance. Neuron 95:928-943 e923.

734 Heine M, Groc L, Frischknecht R, Beique JC, Lounis B, Rumbaugh G, Huganir RL, Cognet L,
735 Choquet D (2008) Surface mobility of postsynaptic AMPARs tunes synaptic
736 transmission. Science 320:201-205.

737 Hirai H, Sakaba T, Hashimotodani Y (2022) Subcortical glutamatergic inputs exhibit a Hebbian
738 form of long-term potentiation in the dentate gyrus. Cell Rep 41:111871.

739 Hnasko TS, Edwards RH (2012) Neurotransmitter corelease: mechanism and physiological
740 role. Annu Rev Physiol 74:225-243.

741 Ito HT, Moser EI, Moser MB (2018) Supramammillary Nucleus Modulates Spike-Time
742 Coordination in the Prefrontal-Thalamo-Hippocampal Circuit during Navigation.
743 Neuron 99:576-587 e575.

744 Jackman SL, Beneduce BM, Drew IR, Regehr WG (2014) Achieving high-frequency optical
745 control of synaptic transmission. J Neurosci 34:7704-7714.

746 Kamondi A, Acsady L, Wang XJ, Buzsaki G (1998) Theta oscillations in somata and dendrites
747 of hippocampal pyramidal cells in vivo: activity-dependent phase-precession of action
748 potentials. Hippocampus 8:244-261.

749 Kesner AJ, Mozaffarilegha M, Thirtamara Rajamani K, Arima Y, Harony-Nicolas H,
750 Hashimotodani Y, Ito HT, Song J, Ikemoto S (2023) Hypothalamic Supramammillary
751 Control of Cognition and Motivation. J Neurosci 43:7538-7546.

Kim S, Sabatini BL (2023) Analytical approaches to examine gamma-aminobutyric acid and glutamate vesicular co-packaging. Frontiers in Synaptic Neuroscience 14.

Kim S, Wallace ML, El-Rifai M, Knudsen AR, Sabatini BL (2022) Co-packaging of opposing neurotransmitters in individual synaptic vesicles in the central nervous system. Neuron 110:1371-1384 e1377.

Kirk IJ, McNaughton N (1991) Supramammillary cell firing and hippocampal rhythmical slow activity. Neuroreport 2:723-725.

Kocsis B, Vertes RP (1994) Characterization of neurons of the supramammillary nucleus and mammillary body that discharge rhythmically with the hippocampal theta rhythm in the rat. J Neurosci 14:7040-7052.

Konno K, Yamasaki M, Miyazaki T, Watanabe M (2023) Glyoxal fixation: An approach to solve immunohistochemical problem in neuroscience research. Sci Adv 9:eadf7084.

Lee S, Kim K, Zhou ZJ (2010) Role of ACh-GABA cotransmission in detecting image motion and motion direction. Neuron 68:1159-1172.

Li Y, Bao H, Luo Y, Yoan C, Sullivan HA, Quintanilla L, Wickersham I, Lazarus M, Shih YI, Song J (2020) Supramammillary nucleus synchronizes with dentate gyrus to regulate spatial memory retrieval through glutamate release. Elife 9.

Ma S, Hangya B, Leonard CS, Wisden W, Gundlach AL (2018) Dual-transmitter systems regulating arousal, attention, learning and memory. Neurosci Biobehav Rev 85:21-33.

Magee JC (2001) Dendritic mechanisms of phase precession in hippocampal CA1 pyramidal neurons. J Neurophysiol 86:528-532.

Markwardt SJ, Wadiche JI, Overstreet-Wadiche LS (2009) Input-specific GABAergic signaling to newborn neurons in adult dentate gyrus. J Neurosci 29:15063-15072.

Neher E, Brose N (2018) Dynamically Primed Synaptic Vesicle States: Key to Understand Synaptic Short-Term Plasticity. Neuron 100:1283-1291.

Nusbaum MP, Blitz DM, Swensen AM, Wood D, Marder E (2001) The roles of co-transmission in neural network modulation. Trends Neurosci 24:146-154.

Pedersen NP, Ferrari L, Venner A, Wang JL, Abbott SBG, Vujovic N, Arrigoni E, Saper CB, Fuller PM (2017) Supramammillary glutamate neurons are a key node of the arousal system. Nat Commun 8:1405.

782 Robert V, Therreau L, Chevaleyre V, Lepicard E, Viollet C, Cognet J, Huang AJ, Boehringer
783 R, Polygalov D, McHugh TJ, Piskorowski RA (2021) Local circuit allowing
784 hypothalamic control of hippocampal area CA2 activity and consequences for CA1.
785 Elife 10.

786 Root DH, Mejias-Aponte CA, Zhang S, Wang HL, Hoffman AF, Lupica CR, Morales M (2014)
787 Single rodent mesohabenular axons release glutamate and GABA. Nat Neurosci
788 17:1543-1551.

789 Root DH, Zhang S, Barker DJ, Miranda-Barrientos J, Liu B, Wang HL, Morales M (2018)
790 Selective Brain Distribution and Distinctive Synaptic Architecture of Dual
791 Glutamatergic-GABAergic Neurons. Cell Rep 23:3465-3479.

792 Rost BR, Wietek J, Yizhar O, Schmitz D (2022) Optogenetics at the presynapse. Nat Neurosci
793 25:984-998.

794 Sakaba T (2008) Two Ca(2+)-dependent steps controlling synaptic vesicle fusion and
795 replenishment at the cerebellar basket cell terminal. Neuron 57:406-419.

796 Schmidt-Hieber C, Jonas P, Bischofberger J (2004) Enhanced synaptic plasticity in newly
797 generated granule cells of the adult hippocampus. Nature 429:184-187.

798 Shabel SJ, Proulx CD, Piriz J, Malinow R (2014) Mood regulation. GABA/glutamate co-
799 release controls habenula output and is modified by antidepressant treatment. Science
800 345:1494-1498.

801 Silm K, Yang J, Marcott PF, Asensio CS, Eriksen J, Guthrie DA, Newman AH, Ford CP,
802 Edwards RH (2019) Synaptic Vesicle Recycling Pathway Determines Neurotransmitter
803 Content and Release Properties. Neuron 102:786-800 e785.

804 Soussi R, Zhang N, Tahtakran S, Houser CR, Esclapez M (2010) Heterogeneity of the
805 supramammillary-hippocampal pathways: evidence for a unique GABAergic
806 neurotransmitter phenotype and regional differences. Eur J Neurosci 32:771-785.

807 Sudhof TC (2013) Neurotransmitter release: the last millisecond in the life of a synaptic vesicle.
808 Neuron 80:675-690.

809 Tabuchi E, Sakaba T, Hashimotodani Y (2022) Excitatory selective LTP of supramammillary
810 glutamatergic/GABAergic cotransmission potentiates dentate granule cell firing. Proc
811 Natl Acad Sci U S A 119:e2119636119.

812 Takacs VT, Cserep C, Schlingloff D, Posfai B, Szonyi A, Sos KE, Kornyei Z, Denes A, Gulyas
813 AI, Freund TF, Nyiri G (2018) Co-transmission of acetylcholine and GABA regulates
814 hippocampal states. Nat Commun 9:2848.

815 Tritsch NX, Granger AJ, Sabatini BL (2016) Mechanisms and functions of GABA co-release.
816 Nat Rev Neurosci 17:139-145.

817 Trudeau LE, El Mestikawy S (2018) Glutamate Cotransmission in Cholinergic, GABAergic
818 and Monoamine Systems: Contrasts and Commonalities. Front Neural Circuits 12:113.

819 Trudeau LE, Hnasko TS, Wallen-Mackenzie A, Morales M, Rayport S, Sulzer D (2014) The
820 multilingual nature of dopamine neurons. Prog Brain Res 211:141-164.

821 Trussell LO, Zhang S, Raman IM (1993) Desensitization of AMPA receptors upon multiquantal
822 neurotransmitter release. Neuron 10:1185-1196.

823 Turecek J, Jackman SL, Regehr WG (2016) Synaptic Specializations Support Frequency-
824 Independent Purkinje Cell Output from the Cerebellar Cortex. Cell Rep 17:3256-3268.

825 Uchigashima M, Yamazaki M, Yamasaki M, Tanimura A, Sakimura K, Kano M, Watanabe M
826 (2011) Molecular and morphological configuration for 2-arachidonoylglycerol-
827 mediated retrograde signaling at mossy cell-granule cell synapses in the dentate gyrus.
828 J Neurosci 31:7700-7714.

829 Vaaga CE, Borisovska M, Westbrook GL (2014) Dual-transmitter neurons: functional
830 implications of co-release and co-transmission. Curr Opin Neurobiol 29:25-32.

831 Wadiche JI, Jahr CE (2001) Multivesicular release at climbing fiber-Purkinje cell synapses.
832 Neuron 32:301-313.

833 Wallace ML, Sabatini BL (2023) Synaptic and circuit functions of multitransmitter neurons in
834 the mammalian brain. Neuron 111:2969-2983.

835 Wallace ML, Saunders A, Huang KW, Philson AC, Goldman M, Macosko EZ, McCarroll SA,
836 Sabatini BL (2017) Genetically Distinct Parallel Pathways in the Entopeduncular
837 Nucleus for Limbic and Sensorimotor Output of the Basal Ganglia. Neuron 94:138-152
838 e135.

839 Wong AY, Graham BP, Billups B, Forsythe ID (2003) Distinguishing between presynaptic and
840 postsynaptic mechanisms of short-term depression during action potential trains. J
841 Neurosci 23:4868-4877.

842 Wu LG, Saggau P (1994) Pharmacological identification of two types of presynaptic voltage-
843 dependent calcium channels at CA3-CA1 synapses of the hippocampus. J Neurosci
844 14:5613-5622.

845 Yoo JH, Zell V, Gutierrez-Reed N, Wu J, Ressler R, Shenasa MA, Johnson AB, Fife KH, Faget
846 L, Hnasko TS (2016) Ventral tegmental area glutamate neurons co-release GABA and
847 promote positive reinforcement. Nat Commun 7:13697.

848 Zucker RS, Regehr WG (2002) Short-term synaptic plasticity. Annu Rev Physiol 64:355-405.

849 Zych SM, Ford CP (2022) Divergent properties and independent regulation of striatal
850 dopamine and GABA co-transmission. Cell Rep 39:110823.
851
852

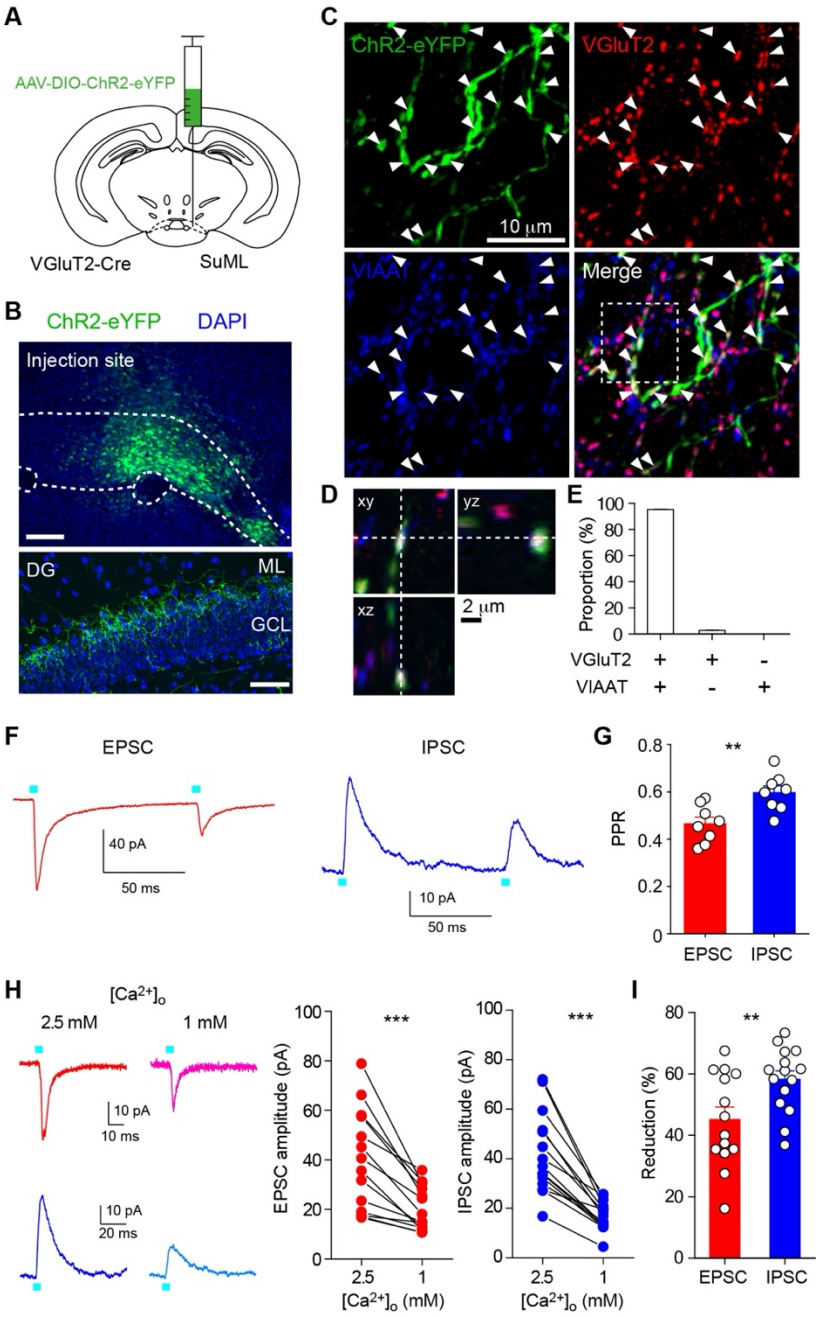

Figure 1. Different PPRs and Ca^{2+} sensitivities of glutamate/GABA co-transmission at SuM-GC synapses

(**A**) Diagram illustrating the injection of AAV-DIO-ChR2(H134R)-eYFP into the lateral part of SuM of VGluT2-Cre mouse. (**B**) (top) Fluorescence image showing the injection site of AAV in the SuM. (bottom) ChR2(H134R)-eYFP-expressing SuM axons are observed in the supragranular layer of the DG. ML, molecular layer; GCL, granule cell layer. Scale bars, Top, 200 μm; Bottom, 50 μm. (**C**) Z-stacked immunofluorescence images double stained for VGluT2 (red) and VIAAT (blue). The merged image demonstrates the colocalization of VGluT2 and VIAAT in the ChR2-eYFP-expressing SuM terminals (arrowheads). (**D**) Higher

magnification xy, xz, and yz projection images outlined in boxed area in (C) show that a SuM bouton is co-stained with VGluT2 and VIAAT. (**E**) Proportion of VGluT2- and/or VIAAT-expressing boutons in the ChR2-eYFP labeled boutons (2205 boutons, 7 slices). Both VGluT2 and VIAAT (95.2 ± 0.3%), VGluT2 only (2.7 ± 0.2%), and VIAAT only (0%). (**F**) Representative traces of EPSC (red, V_h = -70 mV) and IPSC (blue, V_h = 0 mV) evoked with paired pulse illumination (100 ms interval). (**G**) Summary plot of PPR showing a significant difference between EPSC and IPSC. (**H**) Representative traces (left) and summary plots (right) of EPSCs and IPSCs in 2.5 and 1 mM extracellular Ca^{2+}. (**I**) Summary plot of percent reduction in the amplitudes of EPSCs and IPSCs from 2.5 to 1 mM extracellular Ca^{2+}. Data are presented as mean ± SEM. **$p < 0.01$, ***$p < 0.001$.

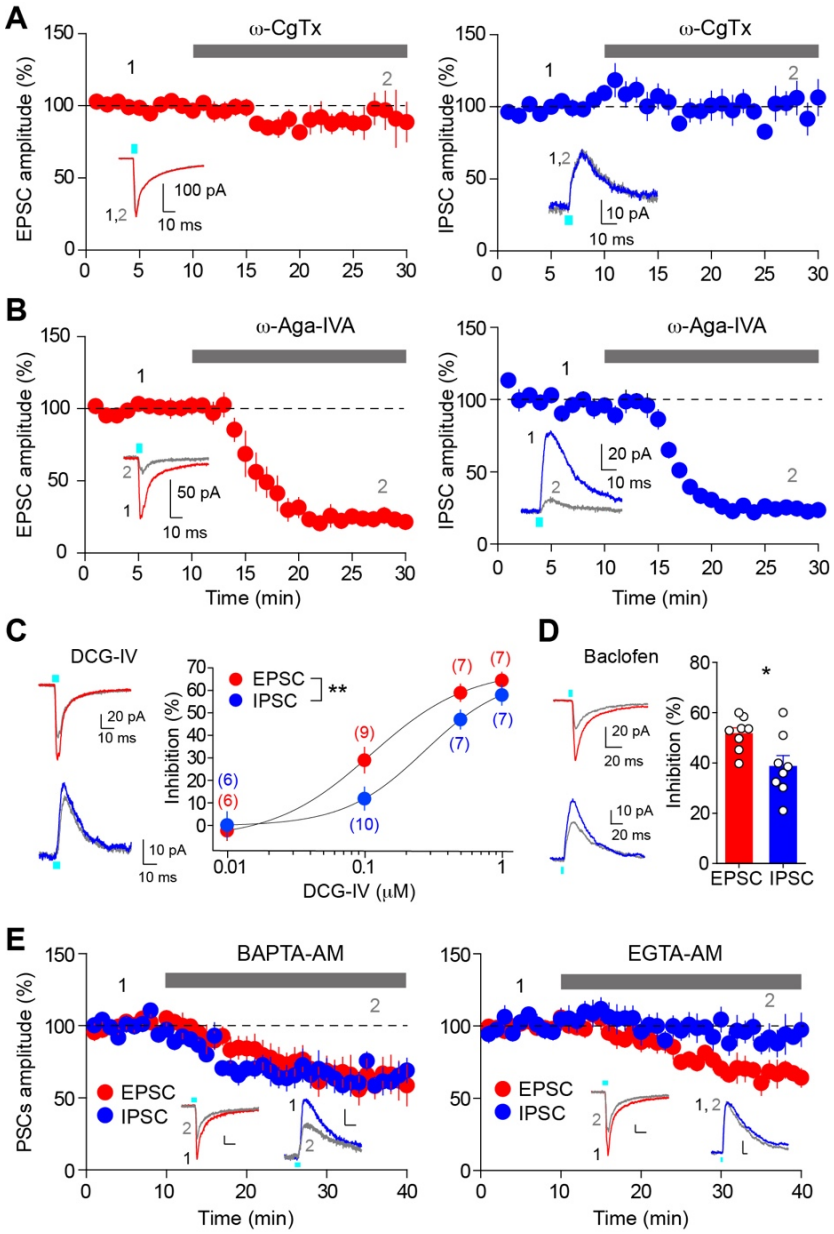

Figure 2. Different presynaptic modulation and Ca^{2+} chelator-sensitivities of glutamate/GABA co-transmission

(**A**) Time course summary plots showing the effects of ω-CgTx (500 nM) on co-transmission of glutamate (left) and GABA (right) at SuM-GC synapses. Insets indicate representative traces. (**B**) Time course summary plots showing that the co-transmission of glutamate (left) and GABA (right) at SuM-GC synapses were inhibited by ω-Aga-IVA (200 nM). Insets show representative traces. (**C**) (left) Representative traces before (EPSC, red; IPSC, blue) and after (gray) application of DCG-IV (0.1 μM). (right) Summary plot of concentration-response curves. Data are fitted to the Hill equation. Numbers in parentheses indicate the number of

941 cells. (**D**) (left) Representative traces before (EPSC, red; IPSC, blue) and after (gray)
942 application of baclofen (5 μM). (right) Summary plot of percent inhibition in the amplitudes
943 of EPSCs and IPSCs by 5 μM baclofen. (**E**) Time course summary plots showing the sensitivity
944 of EPSCs and IPSCs to 100 μM BAPTA-AM (left) and 100 μM EGTA-AM (right). Insets show
945 representative traces. Calibration: 10 pA, 10 ms. Data are presented as mean ± SEM. *$p < 0.05$,
946 **$p < 0.01$.
947

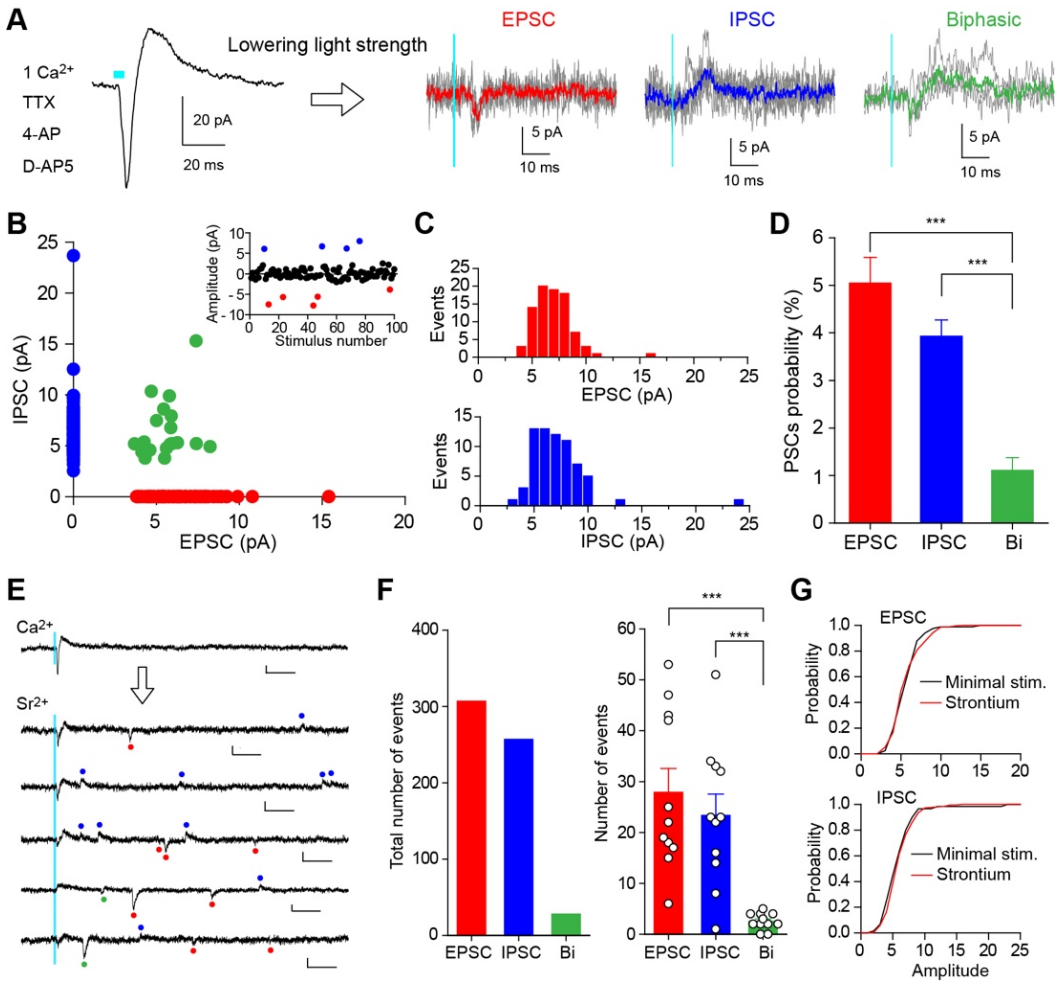

Figure 3. Uniquantal release-mediated synaptic responses evoked by minimal light stimulation or strontium-induced asynchronous release at SuM-GC synapses

(**A**) Representative traces of biphasic response elicited by light stimulation with maximum light power (left) and stochastically evoked PSCs with minimal light stimulation (100 trials for each cell) (right). Synaptic responses at SuM-GC synapses were recorded at holding potentials of -20 to -30 mV in the presence of TTX (1 μM), 4-AP (1 mM), D-AP5 (50 μM), and Ca^{2+} (1 mM). Average EPSC (red), IPSC (blue), and biphasic current (green) are superimposed on individual traces. (**B**) Scatter plot of the amplitude of IPSCs against the amplitude of EPSCs recorded from 17 cells. Success events of 172 PSCs are plotted. (Inset) A single experiment showing 100 trials with an interval of 10 sec elicited stochastically EPSCs (red) and IPSCs (blue). (**C**) Amplitude histograms of EPSCs (top) and IPSCs (bottom) in same data as in B. (**D**) Summary graph of PSCs probability. (**E**) Representative traces showing strontium-induced asynchronous release recorded from GC at holding potentials of -20 to -30 mV. The NMDA receptor antagonist D-AP5 (50 μM) was included in the extracellular solution to eliminate NMDA receptor-mediated EPSCs. Red, blue, and green points indicate detected EPSCs, IPSCs, and

biphasic currents, respectively. Calibration: 10 pA, 50 ms. (**F**) (left) Summary bar graph showing the total number of asynchronous quantal responses (n = 11, 30 trials for each cell) (EPSC: 307 events; IPSC: 257 events; biphasic: 28 events). (right) Averaged number of asynchronous events showing that the majority of asynchronous events are EPSCs and IPSCs, and a few biphasic responses. (**G**) Cumulative distributions of the amplitudes of EPSCs (top) and IPSCs (bottom) for minimal light stimulation-evoked PSCs and strontium-induced PSCs (EPSC: minimal stim.: 86 events from 17 cells; strontium: 307 events from 11 cells, $p = 0.72$; IPSC: minimal stim.: 67 events from 17 cells; strontium: 256 events from 11 cells, $p = 0.096$, Kolmogorov-Smirnov test). Data are presented as mean ± SEM. ***$p < 0.001$.

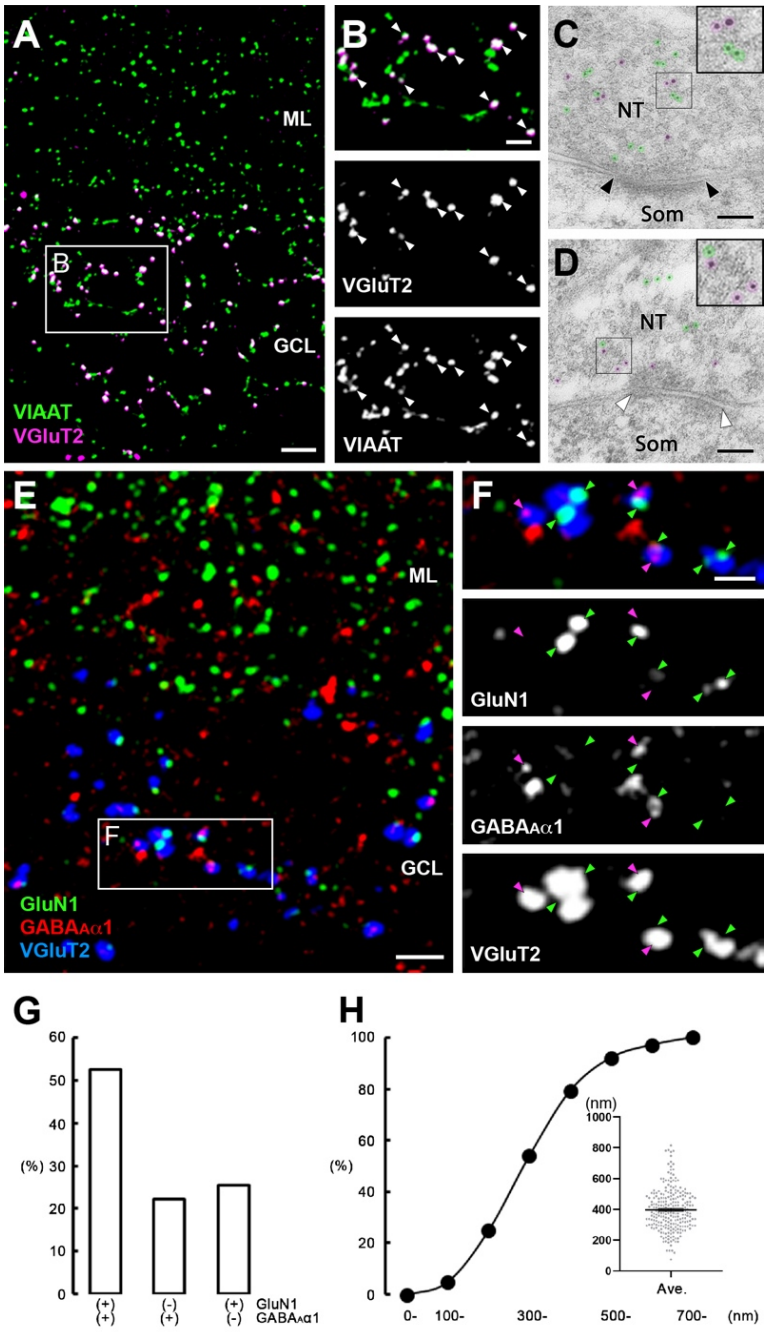

Figure 4. Close association of GluN1 and GABA$_A$α1 facing the same SuM terminals

(**A, B**) Double immunofluorescence for VIAAT (green) and VGluT2 (magenta) in the GC layer of the DG. (B) Higher magnification images of the boxed area in (A) show VGluT2-positive terminals are co-labeled with VIAAT (white arrowheads). (**C, D**) Post-embedding immunogold electron microscopy showing that immunogold particles for VIAAT (magenta, 5 nm) and VGluT2 (green, 10 nm) and are co-exist in the same SuM terminals of asymmetric (C) and symmetric (D) synapses. NT, nerve terminal; Som, soma. (**E, F**) Triple immunofluorescence for GluN1 (green), GABA$_A$α1 (red), and VGluT2 (blue) in the GC layer of the DG. (F) Higher

1034 magnification images of the boxed region in E. Green and magenta arrowheads indicate GluN1
1035 or $GABA_A\alpha1$ puncta that are apposed to VGluT2 puncta, respectively. (**G**) Proportion of
1036 GluN1 and $GABA_A\alpha1$ puncta in close proximity to 634 VGluT2-positive SuM terminals. (**H**)
1037 Cumulative distribution of the distance between GluN1 and $GABA_A\alpha1$ puncta derived from
1038 241 VGluT2-positive SuM terminals that are double-labeled for GluN1 and $GABA_A\alpha1$.
1039 Individual and average values are plotted in inset. Data were obtained from two mice. Scale
1040 bars: A, 5 μm; B, E, 2 μm; C, D, 100 nm; F, 1 μm.
1041

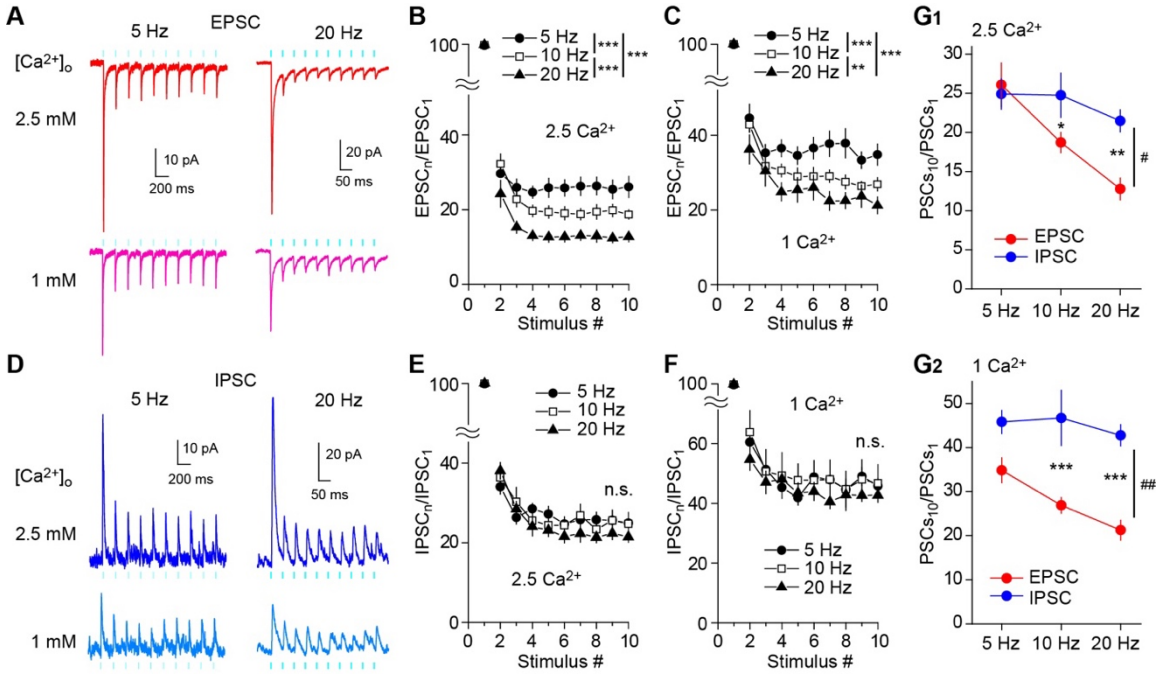

Figure 5. Frequency-dependent shift of glutamate/GABA co-transmission balance of SuM inputs in GCs

(**A, D**) Representative traces of EPSCs (V_h = -70 mV) (A) and IPSCs (V_h = 0 mV) (D) in response to 10 light stimuli at 5 Hz (left) or 20 Hz (right) in 2.5 mM (top) or 1 mM (bottom) extracellular Ca^{2+}. (**B**) Summary graph of normalized EPSC amplitude plotted against the stimulus number in 2.5 mM extracellular Ca^{2+}. Two-way repeated measures ANOVA, $F_{(2,16)}$ = 13.0, $p < 0.001$, n = 9 or 10; Tukey post hoc test: ***$p < 0.001$. (**C**) Same as (B), but recorded in 1 mM extracellular Ca^{2+}. Two-way repeated measures ANOVA, $F_{(2,16)}$ = 11.4, $p < 0.001$, n = 9 or 10; Tukey post hoc test: **$p < 0.01$, ***$p < 0.001$. (**E**) Summary graph of normalized IPSC amplitude plotted against stimulus number in 2.5 mM extracellular Ca^{2+}. Two-way repeated measures ANOVA, $F_{(2,16)}$ = 0.003, p = 0.997, n = 9. (**F**) Same as (E), but recorded in 1 mM extracellular Ca^{2+}. Two-way repeated measures ANOVA, $F_{(2,16)}$ = 0.02, p = 0.981, n = 9. (**G**) Summary plots showing the normalized amplitudes of 10th EPSCs and IPSCs at 5 Hz, 10 Hz, and 20 Hz in 2.5 mM extracellular Ca^{2+} (G1: two-way repeated measures ANOVA, $F_{(1,7)}$ = 8.03, $^{\#}p < 0.05$, n = 9 or 10; Tukey's post hoc test, EPSC versus IPSC, *$p < 0.05$, **$p < 0.01$), or in 1 mM extracellular Ca^{2+} (G2: two-way repeated measures ANOVA, $F_{(1,7)}$ = 21.76, $^{\#\#}p < 0.01$, n = 9 or 10; Tukey's post hoc test, EPSC versus IPSC, ***$p < 0.001$). n.s., not significant. Data are presented as mean ± SEM.

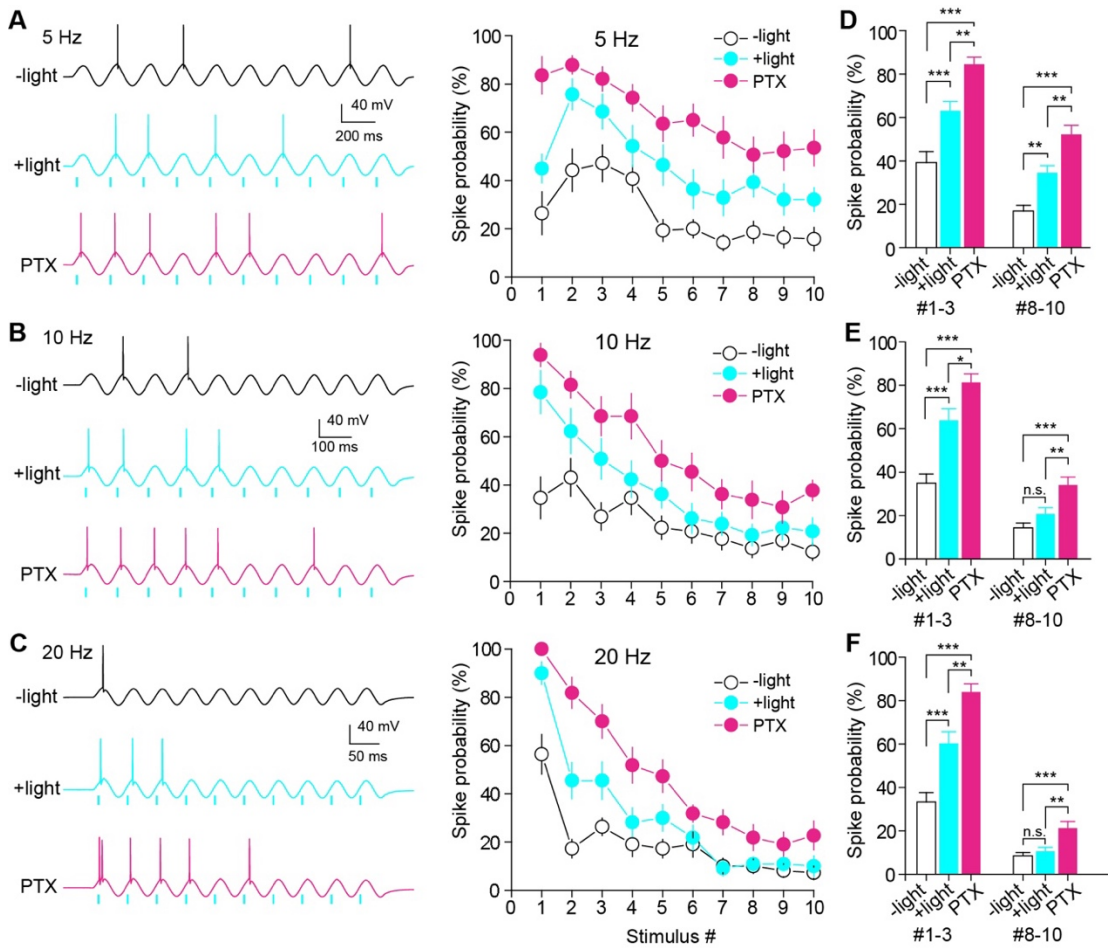

Figure 6. Frequency-dependent modulation of GC firing by SuM inputs

(**A-C**) (left) Representative traces showing GC spikes in response to sinusoidal current injections without (top) and with (middle) paired light stimulation of SuM inputs at 5 Hz (A), 10 Hz (B), and 20 Hz (C). Bottom trace showing the GC response to sinusoidal current injection paired with light stimulation in the presence of 100 μM picrotoxin (PTX). (right) Summary graph of spike probability against stimulus number. (**D-F**) Summary plots of spike probability at initial and last three stimulus numbers at 5 Hz (D), 10 Hz (E), and 20 Hz (F). The spike probabilities of stimulus numbers 1-3 and 8-10 were averaged. (D) one-way ANOVA, n = 14, $F_{(2,123)} = 28.8$, $p < 0.001$ (#1-3), $F_{(2,123)} = 25.8$, $p < 0.001$ (#8-10); Tukey's post hoc test, ***p < 0. 001, **p < 0. 01. (E) one-way ANOVA, n = 13, $F_{(2,114)} = 26.3$, $p < 0.001$ (#1-3), $F_{(2,114)} = 11.8$, $p < 0.001$ (#8-10); Tukey's post hoc test, ***p < 0. 001, **p < 0. 01, *p < 0.05, n.s., not significant. (F) one-way ANOVA, n = 11, $F_{(2,96)} = 31.4$, $p < 0.001$ (#1-3), $F_{(2,96)} = 9.2$, $p < 0.001$ (#8-10); Tukey's post hoc test, ***p < 0. 001, **p < 0.01, n.s., not significant. Data are presented as mean ± SEM.

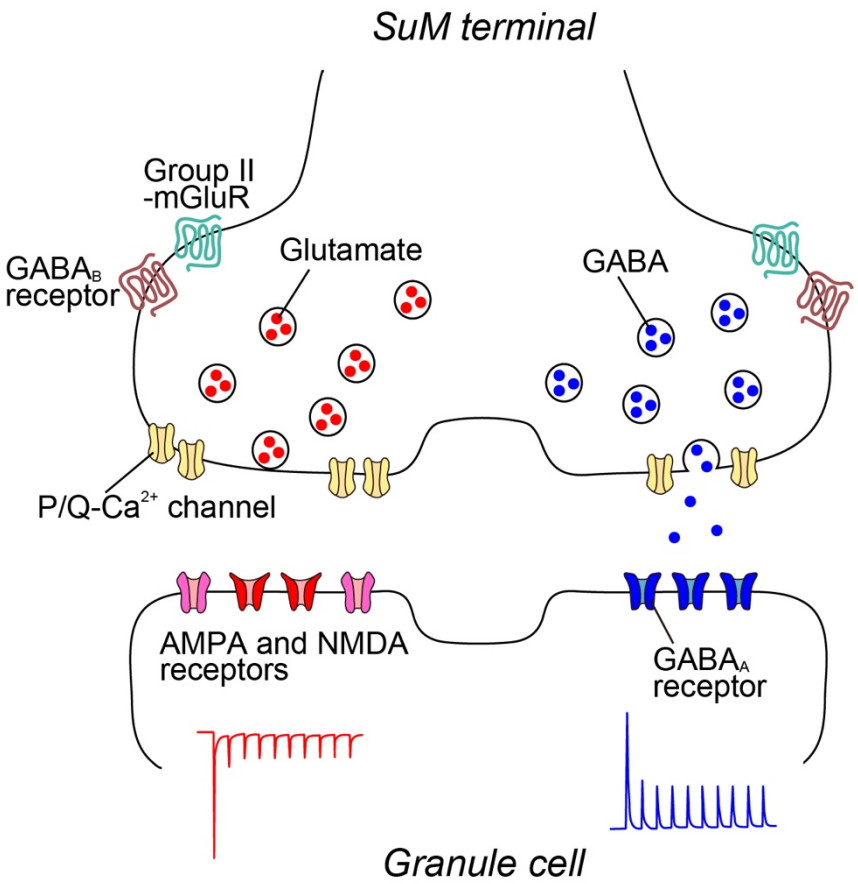

Figure 7. Working hypothesis of synaptic architecture of SuM-GC synapse

A single SuM terminal contains distinct glutamatergic and GABAergic vesicles, which are regulated by P/Q-type Ca^{2+} channels and also modulated by group II mGluRs and $GABA_B$ receptors. Glutamatergic and GABAergic vesicles are loosely and tightly coupled with Ca^{2+} channels, respectively. At the postsynaptic site of GCs, AMPA/NMDA and $GABA_A$ receptors are distributed separately. Based on their molecular composition, glutamatergic and GABAergic synapses are established independently, achieving the distinct glutamatergic and GABAergic transmission.

Supplementary Figures

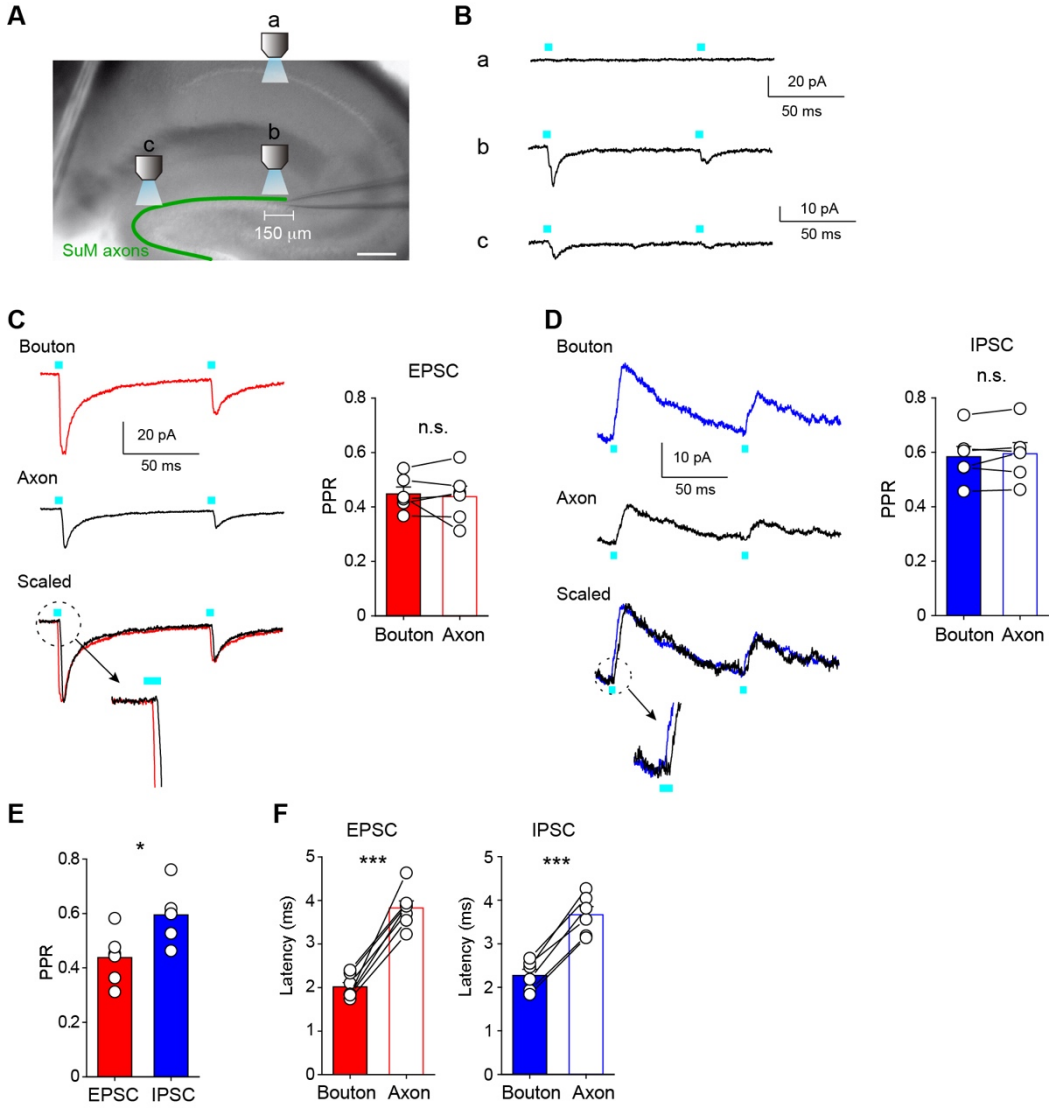

Figure S1. PPRs of glutamatergic and GABAergic co-transmission show no difference between over-axon and over-bouton illumination (Related to Figure 1)

(A) Diagram of the experimental setup. We recorded from GCs located in the most edge of upper blade of GC layer (~150 μm). Once synaptic responses were observed by over-bouton illumination (over-the recorded cell soma, position b), then the objective lens was moved to ~600 μm vertically away in the stratum radiatum of the CA1 region (position a). The light power was adjusted to evoke no response at position a, indicating that SuM-GC synapses on the recorded GCs were out of the illumination field. The objective lens was then returned to position b, and PSCs of SuM-GC synapses were recorded with paired stimulation. Then, the objective lens was moved ~600 μm along the GC layer (position c) to achieve over-axon illumination. Scale bar: 200 μm. **(B)** Representative traces of SuM-GC EPSCs evoked with

over-CA1 (a), over-bouton (b), and over-axon (c) illumination. **(C, D)** Representative traces (left) and summary plots of PPRs (right) of SuM-GC EPSCs (C) or IPSCs (D) indicating no significant difference between over-bouton and over-axon illumination of SuM inputs (EPSC: bouton: 0.45 ± 0.03; axon: 0.44 ± 0.04, $n = 6$, $p = 0.72$, paired t-test; IPSC: bouton: 0.58 ± 0.04; axon: 0.59 ± 0.04, $n = 6$, $p = 0.32$, paired t-test). EPSCs or IPSCs were recorded with over-bouton (top) or over-axon (middle) illumination, respectively. Bottom traces show that a trace by over-axon stimulation was scaled to the peak of a trace by over-bouton stimulation. Magnified traces of the dotted circle show a delayed onset latency of a trace by over-axon stimulation relative to a trace by over-bouton stimulation. **(E)** Summary plot of PPR indicating a significant difference between EPSC and IPSC evoked by over-axon illumination (EPSC: 0.44 ± 0.04; IPSC: 0.59 ± 0.04, $n = 6$, $p < 0.05$, unpaired t-test). **(F)** Summary plots of latency to the onset of the synaptic response. The delayed latency of the synaptic responses by over-axon illumination indicates that synaptic transmission was mediated by light-evoked action potential propagation toward SuM terminals (EPSC: bouton: 2.0 ± 0.1 ms; axon: 3.8 ± 0.2 ms, $n = 7$, $p < 0.001$, paired t-test; IPSC: bouton: 2.3 ± 0.1 ms; axon: 3.7 ± 0.2 ms, $n = 6$, $p < 0.001$, paired t-test). Data are presented as mean ± SEM. *$p < 0.05$, ***$p < 0.001$, n.s., not significant.

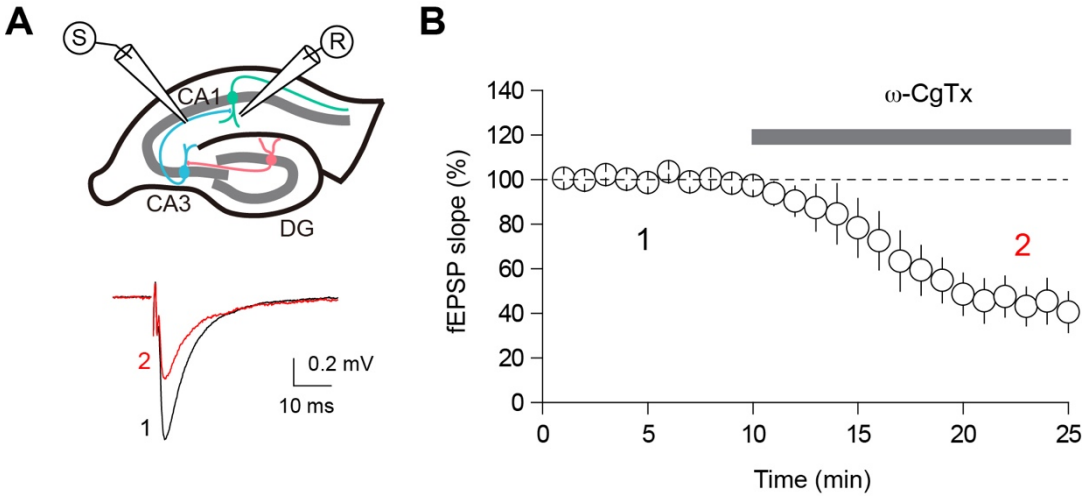

Figure S2. The effect of ω-CgTx on CA3-CA1 transmission (Related to Figure 2)
(**A**) (top) Schematic diagram illustrating the extracellular field excitatory postsynaptic potential recording (fEPSP) configuration. Both the recording and stimulating electrodes were placed in the stratum radiatum of CA1. (bottom) Representative fEPSP traces before (black) and after (red) application of ω-CgTx (500 nM). (**B**) Summary time course plot showing inhibition of CA3-CA1 transmission by ω-CgTx (44.5 ± 9.5% of baseline, $n = 5$, $p < 0.01$, paired t-test). Data are presented as mean ± SEM.

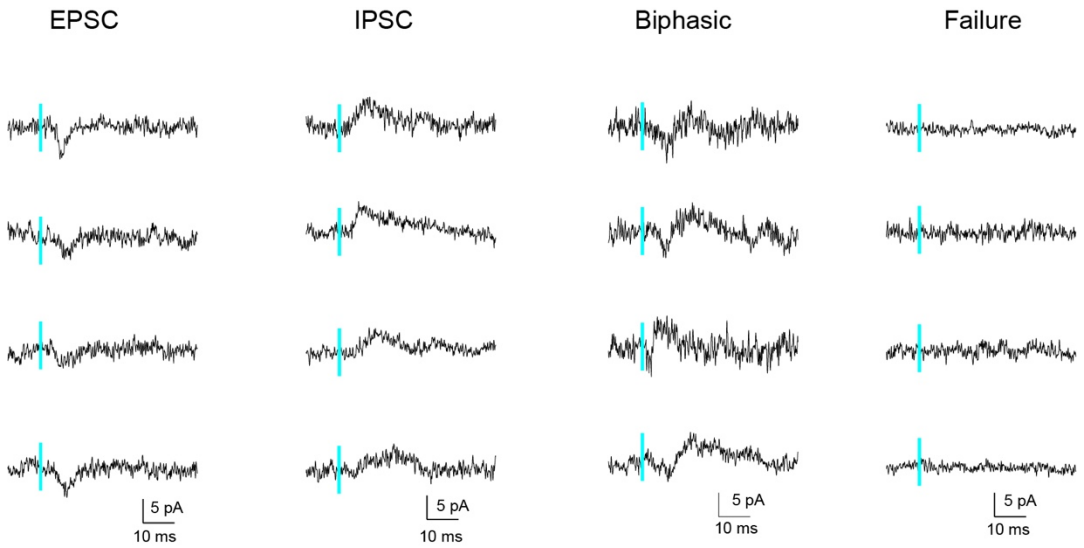

Figure S3. Minimal light stimulation-evoked synaptic responses at SuM-GC synapses (Related to Figure 3)

Sample traces recorded from GCs at holding potential of -20 to -30 mV in response to minimal light stimulation.

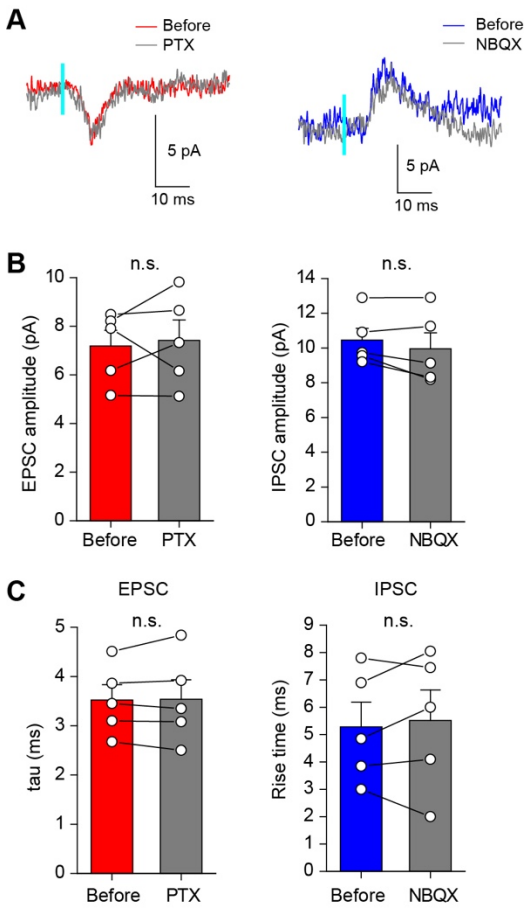

Figure S4. The amplitudes and kinetics of minimal light stimulation-evoked EPSCs or IPSCs at SuM-GC synapses were not altered by blockade of their counterpart currents (Related to Figure 3)

(A) Representative traces of EPSCs (left) and IPSCs (right) evoked by minimal light stimulation of SuM inputs at intermediate membrane potentials. EPSCs or IPSCs were recorded by repeating the light stimulation 100 times before, with the application of 100 μM picrotoxin (PTX) or 10 μM NBQX, respectively. **(B)** Summary plots show that the amplitudes of EPSCs and IPSCs were not changed after application of picrotoxin or NBQX, respectively (EPSC: before: 7.2 ± 0.6 pA; PTX: 7.4 ± 0.8 pA, n = 5, p = 0.71, paired t test; IPSC: before: 10.5 ± 0.7 pA; NBQX: 10.0 ± 0.9 pA, n = 5, p = 0.18, paired t test). **(C)** Summary plots of the decay time constant of EPSCs (tau, single-exponential fit) and rise time of IPSCs (10%-90% of IPSC peak amplitude) (tau: before: 3.5 ± 0.3 ms; PTX: 3.5 ± 0.4 ms, n = 5, p = 0.84, paired t test; rise time: before: 5.3 ± 0.9 ms; NBQX: 5.5 ± 1.1 ms, n = 5, p = 0.60, paired t test). Data are presented as mean ± SEM. n.s., not significant.

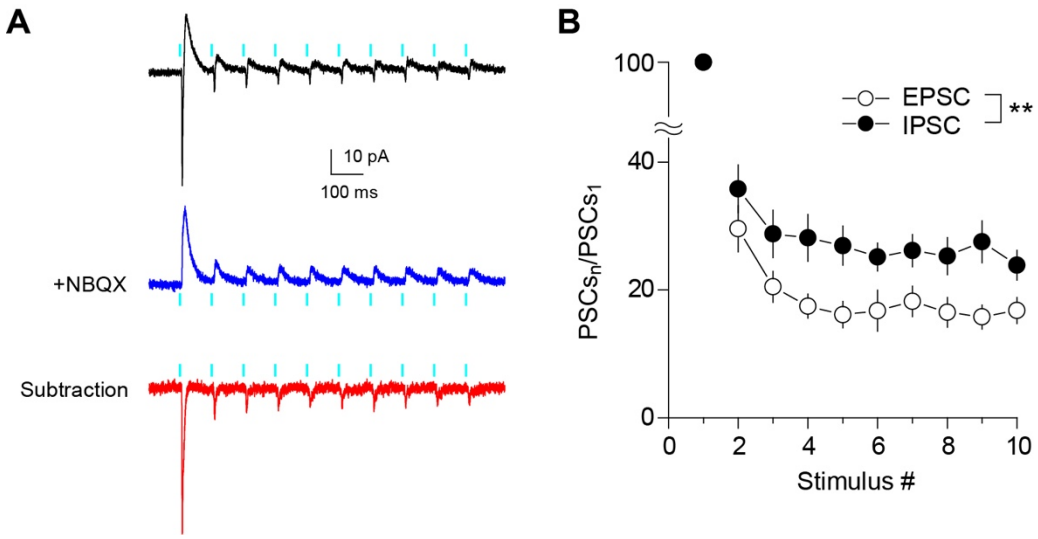

Figure S5. Short-term changes in EPSC/IPSC ratio during train stimulation at SuM-GC synapses (Related to Figure 5)

(**A**) Representative PSCs in response to 10 light pulses at 10 Hz recorded from GC at holding potentials of -30 mV before (black) and after application of 10 μM NBQX (blue). The EPSC (red) was isolated by subtracting the blue trace from the black trace. 1 μM TTX, 500 μM 4-AP, 50 μM D-AP5, 100 μM LY341495, and 3 μM CGP55845 were included in the extracellular solution throughout the experiments. (**B**) Summary graph of normalized EPSC and IPSC amplitudes plotted against stimulus number. Two-way repeated measures ANOVA, $F_{(1,7)} = 17.5$, $p < 0.01$, $n = 8$. Data are presented as mean ± SEM. $^{**}p < 0.01$.

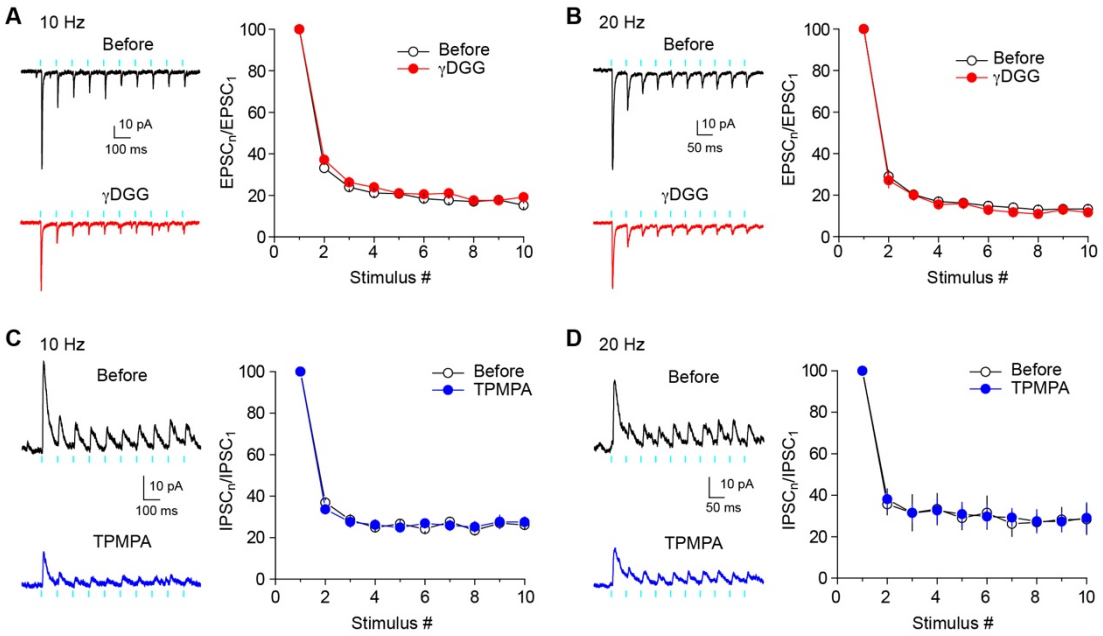

Figure S6. Preventing postsynaptic saturation and desensitization does not alter short-term depression of EPSCs and IPSCs (Related to Figure 5)

(**A and B**) (left) Representative traces showing EPSCs in response to 10 Hz (A) or 20 Hz (B) light stimulation before (top) and after (bottom) application of 2 mM γDGG. (right) Summary graph of normalized EPSC amplitudes plotted against stimulus number. 10 Hz: Two-way repeated measures ANOVA, $F_{(1,7)} = 1.78$, $p = 0.22$, $n = 8$. 20 Hz: Two-way repeated measures ANOVA, $F_{(1,7)} = 0.65$, $p = 0.45$, $n = 8$. (**C and D**) (left) Representative traces showing IPSCs in response to 10 Hz (C) or 20 Hz (D) light stimulation before (top) and after (bottom) application of 300 μM TPMPA. (right) Summary graph of normalized IPSC amplitudes plotted against stimulus number. 10 Hz: Two-way repeated measures ANOVA, $F_{(1,5)} = 1.02$, $p = 0.44$, $n = 6$. 20 Hz: Two-way repeated measures ANOVA, $F_{(1,4)} = 0.21$, $p = 0.67$, $n = 5$. Data are presented as mean ± SEM.

1305 **Table S1. List of primary antibodies used in the present study.**

1306

Molecules	Sequence (NCBI #)	Host	RRID	Specificity	Source	Figure
$GABA_A\gamma2$		Rb	AB_2263066	KD	Synaptic Systems (224003)	Fig. 4
GluN1		Ms	AB_2571605		Millipore (MAB363)	Fig. 4
VGluT2	559–582 aa (BC038375)	Gp	AB_2571621	IB	Miyazaki et al., 2003 (MSFR107440)	Fig. 4
		Go	AB_2571620	IB	Kawamura et al., 2006 (MSFR106270)	Fig. 4
		Rb	AB_2571619	IB	Miyazaki et al., 2003 (MSFR106300)	Fig. 1
VGAT/VIAAT	31–112 aa (BC052020)	Rb	AB_2571622	IB	Miura et al., 2006 (MSFR106120)	Fig. 4
		Gp	AB_2571624	IB	Miura et al., 2006 (MSFR106150)	Fig.1, 4
GFP		Go	AB_305643		Abcam (ab6673)	Fig.1

1307

1308

1309

1310

1311

1312

1313